Near Surface Geophysics, 2014, **12**, 93-115 doi: 10.3997/1873-0604.2013057

Geoelectrical monitoring of frozen ground and permafrost in alpine areas: field studies and considerations towards an improved measuring technology

Robert Supper[1*], David Ottowitz[1], Birgit Jochum[1], Alexander Römer[1], Stefan Pfeiler[1], Stefanie Kauer[1], Markus Keuschnig[2,3] and Anna Ita[1]

[1] *Geological Survey of Austria, Neulinggasse 38, A-1030 Vienna, Austria*
[2] *University of Salzburg / Department of Geography and Geology / Research Group Geomorphology and Environmental Systems*
[3] *AlpS - Centre for Climate Change Adaptation Technologies, Innsbruck, Austria*

Received September 2012, revision accepted November 2013

ABSTRACT

Processes that control permafrost warming in Alpine regions are still not completely understood. Recently, geoelectrical monitoring has emerged as a useful tool to investigate thawing and freezing processes. However, high resistive environments and harsh environmental conditions pose very unfavourable conditions for automated resistivity measurements. Based on the results of several test studies, an improved data acquisition system for geoelectrical monitoring of frozen soils was developed. Furthermore, the implementation of algorithms for statistical analysis of raw data time series led to a significant improvement in the reliability of inversion results. At two Alpine sites, namely Mölltaler Glacier and Magnetköpfl/Kitzsteinhorn, the adapted system was tested at soil temperature conditions between 0°C and –12°C. Data was continuously collected at both locations over nearly a full seasonal cycle. The results showed an almost linear dependency of resistivity and temperature at values above –0.5°C. At lower temperatures, the relation was non-linear, indicating that the reduction of porosity due to the shrinking of connected brine channels was the dominating process that determined the value of resistivity. Based on the derived results, further improvements were suggested, especially for measurements at soil temperatures below –4.5°C as low injection currents make it extremely challenging to gather these.

INTRODUCTION

In the Alpine Region climate warming causes a successive deepening of the active layer of permafrost regions (e.g., Kroisleitner *et al*. 2011). Consequently, mass-wasting processes are encouraged, which may affect even valleys below the periglacial belt. Detailed knowledge about underlying processes is still lacking.

Consequences of permafrost warming include the increase of permafrost creep rates due to the presence of unfrozen water causing a reduction of frictional resistance (French 1996, Hoelzle *et al*. 1998, Ikeda *et al*. 2003), a possible decrease of slope stability (Zimmermann and Haeberli 1992, Matsouka *et al*. 2003, Gruber and Haeberli 2007) and a reduction in rock wall stability (Noetzli *et al*. 2003, Davies *et al*. 2003). As a result, permafrost thawing could produce serious and far reaching environmental and engineering problems in permafrost regions and beyond (Smith 1993, Haeberli *et al*. 1998, Harris *et al*. 2001), causing endangerment of buildings in mountainous areas, e.g. of alpine huts. Therefore, acquiring greater knowledge of freezing and thawing processes in permafrost regions is high priority. The advancement of innovative methods, such as geoelectrical monitoring, allowing all-seasonal, permanent monitoring of remote areas is in demand.

The geoelectrical method determines the distribution of the specific electrical resistivity within the subsurface. The specific electrical resistivity mainly depends on porosity, water saturation, conductivity of pore fluid and clay content, and to a minor extent on particle shape and pore geometry. During the process of permafrost thawing and freezing, the volume fraction of the fluid phase (equivalent to a change in porosity), the connectivity of fluid areas and the salinity of the pore fluid is expected to vary. Therefore, geoelectrical monitoring could be an appropriate tool to investigate such processes.

THE APPLICATION OF GEOELECTRICS IN PERMAFROST MONITORING: A STATE-OF-THE-ART REVIEW

The applicability of the geoelectrical method for permafrost investigations was demonstrated by several authors, e.g. by Kneisel *et al*. (2008), Hauck (2002), Hauck *et al*. (2003), Marescot *et al*. (2003), Vanhala *et al*.(2009), Laxton and Coates

*robert.supper@geologie.ac.at

TABLE 1
Overview on permafrost monitoring activities, described in recent literature (all values to the best of our knowledge).

	Kitzsteinhorn (this paper)	**Mölltaler Glacier (this paper)**	**Schilthorn E-W (Hilbich *et al.* 2011)**	**Zugspitze (Krautblatter 2010)**	**Murtèl (Hilbich *et al.* 2009)**	**Schilthorn (Hilbich *et al.* 2008)**	**Steintälli (Krautblatter 2007)**	**Val Muragl (this issue)**	**Brüeltobel (this issue)**	**Murtèl \ Corvatsch (this issue)**
System	GEOMON^{4D}	GEOMON^{4D}	Geotom (Geolog)	ABEM SAS 300C	Syscal	Syscal	ABEM SAS 300C	Syscal	Syscal	Syscal \ Geotom (Geolog)
Number of electrodes	81	81	30	127; 3 arrays overlapping (41, 61, 41)	48	30	41	36	36	36
Electrode Type	Stainless Steel	Stainless Steel	Stainless Steel	Stainless Steel	Stainless Steel	n/a	Stainless Steel Screws	Stainless Steel	Stainless Steel	Stainless Steel
Spacing	1 m	1 m	2 m	1.53 m, 4.6 m, 1.53 m	5 m	2 m	1.5 m	1m, 2m	1.8 m	2 m
Profile length	80 m	80m	58 m	276 m	235 m	60 m	60 m	35 m	63 m	70 m
Configuration	Gradient	Gradient	Wenner, Wenner-Schlumberger, Dipole-Dipole	Wenner, Schlumberger, Gradient	Wenner	Wenner	Wenner	Wenner, Schlumberger	Wenner, Dipole-Dipole	Wenner
Number of data sets	544 (at date 29.3.2013)	250	180	7	4	110	4	20	16	5\58
Number of data points	2600	2600	135	1550	n/a	135	190	n/a	n/a	n/a
Frequency of Measurements	daily	daily	daily since April 2009 (summer 3, winter 2 per day)	once per month in February, May, June, July, August, September, and October 2007	sporadic; at least one measurement every Aug./Sept.	variable, yearly, with some monthly and daily periods	sporadic, August - September	annually - snowfree period	4-8 times a year (weekly)	sporadic \ daily
Observation Period	10/2011-2013	9/2010-9/2011	04/2009-04/2010 with some breaks	February - October	2006-2008	1999-2006	summer 2005	2005-2009	2009-2011	Aug. 2010-Feb. 2011 \ Mar. - Jun. 2011
Current range [mA]	0.001-2	0.03-2	0.001-200	> 0.2	0.02-2	n/a	> 0.2	n/a	n/a	n/a
Resistivity range [kOhmm]	50-1500	1-200	0.6-3.5	1-2000	10-1000	1-2	1-80	1-25	1-1000	2-300
Contact resistance	n/a	n/a	< 10 kΩ	1-100 Ω	up to 500 kΩ	n/a	n/a	3-40 kΩ	5->400 kΩ	20-500 kΩ
Data error estimation	raw data statistics	data statistics	Filtering, de-Spiking of app. Res.	reciprocity principle Slater *et al.* 2000)	DOI index (Oldenburg and Li 1999)	n/a	n/a	n/a	n/a	n/a
RMS error	4-25%	3-26%	3%	10-20 %	4-5 %	2-4 %	6-18 %	2-3 %	2.2-15 %	2.5-8.5 %
Inversion software	EarthImager	EarthImager	Res2DInv	CRTomo (Kemna 2000)	Res2DInv	Res2Dinv	Res2DInv	Res2DInv	Res2DInv	Res2DInv
Active layer thickness	n/a	n/a	5 m	n/a	4-7m	5 m	2-6 m	5 m	1 m	2 m
min. Temperature (-1 m)	-12°C	-7.5°C	-1.5°C	-4°C	no successful measurements in winter	-3°C	only summer	-0.85°C	-8.5°C	-0.8°C

(2010), Oldenborger (2010), Rödder and Kneisel (2012) and Lewkowicz *et al*. (2011). Some recent papers also describe the application of geoelectrics for repeated measurements of the same profile at different seasonal periods (e.g., Sass 2004, Krautblatter and Hauck 2007, Ribolini and Fabre 2007, Noetzli *et al*. 2008, Hilbich *et al*. 2009, Schneider *et al*. 2011). E.g. Hilbich *et al*. (2008) presented a 7-year monitoring study, using electrical resistivity tomography and thermal monitoring at Schilthorn. Almost all authors stress the importance of developing advanced algorithms to estimate data errors. For this purpose Hilbich *et al*. (2009) used the DOI index technique (Oldenburg and Li 1999), whereas Krautblatter *et al*. (2010) suggest the

reciprocity principle (Slater *et al*. 2000). However, publications about permanent geoelectrical installations with at least daily measurements over a longer period are very scarce (Table 1). Although several test studies are reported to be taking place or to have commenced at the time of writing (pers. comm.), the only published case study known to us is the one by Hilbich *et al*. (2011). They describe the results from a one year monitoring period at Schilthorn, with a measurement rate of several sections per day, obtained with an automated Geotom multi-electrode resistivity instrument.

Table 1 gives an overview of the major parameters of recently published permafrost monitoring attempts, including selected major publications describing the results from repeated measurements and the results from this paper for comparision. The table shows that, except for the Schilthorn site where only resistivities below 2 kΩm were detected, subsurface resistivities could range from 1 kΩm to values as high as several MΩm. In such cases, only currents between 0.2 and 0.02 mA could be injected. It is also interesting to note that at all previous sites, minimum soil temperatures were above –4°C and that at all sites (except Schilthorn), measurements were only performed during the spring, summer and autumn seasons, when most probably the surface layer was not frozen. Thus, measurements were most probably performed at times when a significant amount of connected brine channels in the subsurface were still available. Hence, problems related to bad electrode contact due to freezing of electrodes could be minimized. Moreover, it seems that the Schilthorn site represents an exceptional case, with very favourable parameters for geoelectrical monitoring (low contact resistances, low resistivity values), but is, in comparison to other test sites, rather unusual as a permafrost monitoring site.

Recently some work was also done on capacitive coupled measurements, which could help to minimize the influence of high contact resistivities on the geoelectrical results. Hauck and Kneisel (2006) compared a capacitively-coupled AC resistivity system and a standard galvanically-coupled DC multi-electrode resistivity system in terms of permafrost detection. Kuras *et al*. (2011) applied Capacitive Resistivity Imaging (CRI), a low-frequency, capacitively-coupled measurement approach, in order to emulate ERT without the need for galvanic contact on frozen ground. A prototype instrumentation was developed and applied to laboratory experiments, simulating permafrost growth, persistence and thaw in bedrock.

At the Geological Survey of Austria, research for geoelectrical permafrost monitoring was started in 2006 with the adaptation of the geoelectrical monitoring system Geomon^{4D}, followed by several field tests at the Sonnblick observatory, on frozen lakes and in ice caves (Supper *et al*. 2010, Hausmann *et al*. 2010).

To conclude, the review of literature documented that several attempts have been made in recent years to complete tests in geoelectrical permafrost monitoring. However, hardly any complete time series for whole seasonal cycles exist and most tests were performed at comparatively "high" subsurface temperatures (>–4°C). Moreover, published research results show that conventional geoelectrical instrumentation and inversion must be adapted to suit the special requirements of permafrost monitoring.

THE ELECTRICAL CONDUCTIVITY OF FROZEN SOIL AND ICE

Review of the theoretical background

For most sediments and rocks we can assume that the rock matrix (excluding clay fractions) does not contain any conductive material and therefore the electrical conductivity is determined by the electrolytic conduction of fluids present within the pore space or inside fractures. Consequently, the DC conductivity of porous or fractured subsurface matter depends on porosity, saturation of the pore space and conductivity of the pore fluid, as well as on the connectivity of possible migration paths, their tortuosity and clay content.

Under standard conditions, water freezes at 0°C. For salt solutions, however, the situation is different. Where the salt concentration of the initial liquid is below the eutectic composition, ice forms progressively during freezing. The residual liquid then becomes more saline until the eutectic temperature is reached, at which point the remaining liquid suddenly freezes to the eutectic composition of ice and salt hydrate (Stillmann *et al*. 2010, Marion and Grant 1994). Above the eutectic temperature (–4.15°C for $MgSO_4$, –21.2°C for NaCl and –51.15°C for $CaCl_2$; Grimm *et al*. 2008) as temperature decays, ice interlayers first begin to form in the central portions of water filled pores (Derjaguin and Churaev 1978) and connected brine channels, responsible for static (DC) conductivity, developing around the ice nuclei, provided that the initial concentration of the solution is above 3 mM (Grimm *et al*. 2008). A concentration of 3 mM is equivalent to approximately 333 mg/l of $CaCl_2$, 175.2 mg/l of NaCl and 360 mg/l of $MgSO_4$, a concentration usually found in mineral waters. To calculate the DC conductivity, Archie's Law (Archie 1942) can still be applied (factor $m \approx 2$; Grimm *et al*. 2008), highlighting the non-linear relationship between unfrozen water content and DC conductivity. Below this threshold, brine exists inside isolated brine pockets and therefore does not contribute to DC conductivity. Some measurements of the authors showed that pore fluids of Alpine permafrost soils usually have very little mineralization because they originate directly from precipitation or snow melt, although there is a lack of detailed studies on this. Therefore we assume that the latter situation will prevail. Consequently, in such a case the DC conductivity is solely determined by the conductivity of the comprised ice, which is based on protonic point defects in the hydrogen-bounded ice lattice (see below for further description) and is orders of magnitudes lower (approximately 10^{-8} Sm^{-1} at –10°C to 10^{-10} Sm^{-1} at –40°C; Grimm *et al*. 2008). Only at temperatures very close to 0°C, might connected channels exist. Laboratory measurements also showed that in substrate with pore diameters less

than one micrometre, connected brine channels could not develop. However, for clay-like substrates, e.g. montmorillonite, an enhanced DC conductivity (almost three orders of magnitudes higher than other substrates with comparable specific surface area) was found, attributed to surface charge (cation) and/or proton mobility in thin films of H_2O within swelling clay interlayers (Stillmann *et al*. 2010).

Similarly, several other authors report that as freezing continues, mobile ions can also be found in continuous thin films of unfrozen, interfacial water, lining the soil particle pores (Murrmann 1973, Moore and Maeno 1993). Their thickness depends on the surface forces of the substrate (Derjaguin and Churaev 1986) and decreases with temperature. Moore and Maeno (1993) reported that soils with only ice-hydrophobic boundaries contain mobile molecules until temperatures reach –15°C to –20°C, whereas in systems with ice-hydrophilic boundaries, mobile ions can be found even at temperatures between –50°C and –100°C. The special structure and behaviour of very thin films is very different from that of water in bulk (Derjaguin and Churaev 1978) and therefore involved processes are quite complex. Further details on processes and the calculation of ice/free water proportions are given by Derjaguin and Churaev (1986), Komarow (2003), Lukin *et al*. (2008) and Komarov *et al*. (2012), whereas Frolov (2003) developed a complex macrosystem model of frozen ground.

As stated above, where there is sub-eutectic composition, conductivity sharply decreases when cooling below the eutectic temperature takes place. Below the eutectic temperature, and assuming initial conditions below eutectic composition, segregated ice is surrounded by the eutectic mixture of ice and hydrate, whereas hydrate seems to be connected (Grimm *et al*. 2008). DC conductivity is then dominated by the conductivity of the hydrates, which is based on the same principles as that of massive ice (i.e., protonic point defects and migration of protons through the lattice), but is much higher.

Hobbs (1974), Glen (1974, 1975), Glen and Paren (1975), Petrenko (1993), Wolff et al. (1997), Petrenko and Withworth (1999) and De Koning and Antonelli (2007) gave very comprehensive reviews on the electrical properties of massive ice. Petrenko (1993) focused on the theory of Jaccard (1959) to explain the empirically derived properties of ice. This model is based upon the concept of two different types of charge carriers, namely ionic (H_3O^+ and OH^- ions) and Bjerrum defects (L- and D-defects), and changes occurring in the ice structure due to the motion of these defects, triggered by thermoactivation. Additionally, impurities (HF, HCl, NH_3, KOH, NaOH, KCl, NH_4F) can drastically change the protonic carrier concentration. He further reported that ice shows a static (DC) conductivity (σ_S) and a high-frequency conductivity (σ_∞). The first one is three orders of magnitude lower, since for static (DC) conduction majority charge carriers (intrinsic Bjerrum defects for pure ice) as well as minority charge carriers (intrinsic ionic defects) are required to move. Therefore, the latter dominates DC conduction (Grimm *et al*. 2008). The transition frequency, called Debye frequency, is temperature dependent and changes from 10^5 Hz (0°C) to zero at low temperatures (Petrenko 1993). If a steady electric field is applied to ice, the frequency dependence generates an unusual time dependency of the electric current through it, which can be approximated by an exponential decrease from E σ_∞ to the constant value E σ_S.

Figure 1a (compiled after Grimm *et al*. (2008) and Stillman *et al*. (2010)) demonstrates the characteristic temperature dependency of different material. Sand and impure ice with a high ion concentration of 100 mM clearly show an abrupt increase of resistivity below the eutectic temperature, being indicative for brine channel conductivity. For sand and impure ice at a concentration of 1 mM as well as for montmorillonite in general, this change is not apparent. This might be due to a lack of connected brine channels, even above the eutectic temperature. At 1mM resistivities in general are much higher than at 100 mM. The lower resistivity of sand, compared to that of impure ice at 1 mM, might be due to an additional conductivity along thin liquid water layers lining soil particles. This effect is even more dominating for montmorillonite, which shows a much lower resistivity at 1 mM compared to impure ice and sand.

Implications for permafrost monitoring

For permafrost measurements in the Alpine area a limited temperature range can be assumed. Based on the available data from Magnetköpfl/Kitzsteinhorn (most of the time no snow cover), the minimum temperature at 0.8 m depth was around –12°C, whereas at Sonnblick (thick snow cover during winter, Fig. 1b) –7°C could be recorded at 1 m depth, and –2.5°C at 7 m depth. This range is indicated as shaded area in Fig. 1a. Consequently, based on the result from Fig. 1a and assuming a concentration of 1mM, (which seems to be realistic for most areas as upper value), we can expect a resistivity between 0.5 and 10 kΩm for montmorillonite, 500–200 kΩm for saturated sand and 60 kΩm to 2 MΩm for impure ice. For temperatures close to 0°C, partial melting, super-cooling and/or the development of brine channels takes place even at low ion concentrations.

The findings from our literature study suggest several problems for permanent geoelectrical monitoring installations on frozen ground. One arises from the **exponential time dependency of the electric current** after the start of the injection. Hence, the application of a constant voltage might result in a variable injection current. Therefore we have to introduce a sufficient time delay between the start of the current injection and potential data sampling in order to allow the stabilization of the input current, or to adjust the current also during potential sampling by changing the applied voltage.

According to Petrenko (1993) further attention has to be put on **the proper contact between electrode material and soil.** Usually metal electrodes, like stainless steel, are used. Since metals are electronic conductors and ice is a protonic conductor, it is difficult to ensure efficient charge exchange. This might have

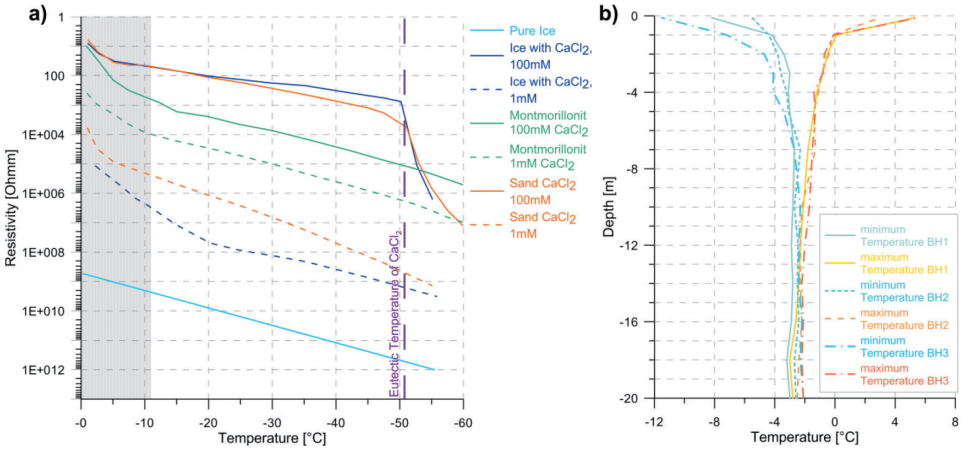

FIGURE 1
a) Resistivity of pure ice, impure ice, clay and sand (based on data published by Grimm *et al.* 2008 and Stillman *et al.* 2010); b) Maximum and minimum temperatures recovered over one year at 3 drill holes close to the Sonnblick observatory (3106 m a.s.l.), data kindly provided by the Central Institute of Meteorology and Geodynamics (ZAMG).

significant effects for current injection into the subsurface. First of all, it could be difficult to ensure a stable DC flow through the metal/ice interface.

Secondly, current flow has to be high enough to obtain a sufficient signal-to-noise ratio for accurate potential difference measurements.

For long time monitoring applications, **electrolytic decomposition of ice** at electrode surfaces could also cause severe problems when low DC voltages (6–30 V) are applied. At the contact surface between ice and the metal electrode, sublimation occurs and a nonconductive gas layer is built, and consequently the bound is eliminated. The approximate response time for these processes is in the range of minutes (Petrenko and Qi 1999, Petrenko and Courville 2000, Haehnel 2001).

Another important issue is related to the question, if and how **ice temperature and structure is changed** due to the repeated injection of direct current. Petrenko and Ryzhkin (2011) showed that a DC current, applied to ice, causes Joule and non-Joule heating, in some special cases also non-Joule cooling, whereas the effect of non-Joule processes is larger at deeper temperatures. However, the whole effect is very short-lived (Petrenko and Ryzhkin 2011) and partially equalized by the reversed current injection.

Further problems emerge during the start of the thawing period. At that time a very thin but conductive surface layer could develop, which acts as a preferential flow path for a **short-cut current** along the soil surface directly between electrodes. Since its conductivity can be much higher than brine channel conductivity (Caranti and Illingworth 1983, Petrenko and Ryzhkin 1997, Khusnatinov *et al.* 1997) and the layer thickness is very low, it cannot be handled by conventional inversion routines, thus producing inversion artifacts.

The findings above imply that permafrost monitoring by geoelectrical measurements could encounter several difficulties, which have to be taken into account when designing a proper measuring technique. Apart from that, additional challenges are posed by the measurement of very high resistivities, the operation of a system at very remote locations and at very deep temperatures, and the selection of a robust and long lasting power supply.

DEVELOPMENT OF AN IMPROVED MEASURING TECHNOLOGY FOR PERMAFROST MONITORING

Measurement of ERT profiles in highly resistive environment – considerations regarding limiting parameters of available DAQ systems

Conventional geoelectrical surveys are usually carried out in geological environments exhibiting resistivities between 1 and 5000 Ωm. Therefore, commercially available instruments (Table 2) were traditionally optimised for this range of values. Within this resistivity range, a maximum input voltage range of +/– 10 V is usually sufficient to take reliable measurements. Therefore this represents the upper input limit implemented in most commercial systems. As Table 2 shows, only the recent generation of some instruments have higher input ranges. This limitation could cause crucial problems for the measurement of permafrost related phenomena, as will be shown in the following chapter.

In frozen soil we typically encounter resistivities between 10 kΩm and 3 MΩm. Traditionally several different electrode arrays are used for geoelectrical exploration (Dahlin and Zhou 2004). For theoretical evaluation of the expected measuring response at the potential input channel of the instrument, we will focus on the Wenner configuration, one of the most commonly applied array types. The Wenner array is a special case of the Schlumberger array (with equally spaced electrodes), which is in turn the special, symmetrical form of the gradient array. For simplicity, we assume the subsurface to be a homogenous halfspace with a constant resistivity. Its values will be varied from 500 Ωm to 10 MΩm. With this assumption, the calculated apparent resistivity ρ_{app} is equal to the true bulk resistivity of the subsurface.

The apparent resistivity, ρ_{app} is calculated as (Koefoed 1979)

$$\rho_{app} = 2^{*}\,\pi^{*}a^{*}R_{meas} \tag{1}$$

$$R_{meas} = \frac{U_{meas}}{I_{inj}}$$

TABLE 2
Technical specifications of common geoelectrical DAQ instruments (to the best of our knowledge).

	STINGTM	SuperStingTM	SYSCAL R2	SYSCAL Pro	TERRA METER SAS 300C	TERRA METER LS	GEOTOM	GEOMON^{4D}	GEOMON^{4D}-II
Measurement principle	dc time series averaging	dc time series averaging	dc time series averaging	dc time series averaging	dc time series averaging	dc time series / averaging	lock-in amplifier	dc time series	dc time series
Output current waveform	rectangle	rectangle	rectangle	rectangle	rectangle	rectangle	sinus	rectangle	rectangle
source principle	const. current	const. voltage	const. voltage	const. voltage	const. current	const. current	const. current	const. current	const. current
Input impedance	> 20 M Ohm	> 150 M Ohm	> 10 M Ohm	> 100 M Ohm	> 10 M Ohm	> 200 M Ohm / 300 k Ohm	> 20 M Ohm	> 20 M Ohm	> 200 M Ohm
Power	200 W	200 W/15 kW	250/1200 W	250/1200 W	4/200 W	250 W	70 W	380 W	380 W
Current sensor resolution	1 mA	<1 μA	10 μA	4 μA	n/a	n/a	1 μA	10 μA single measurements, <2 μA averaging	< 1 μA
Current range	1 - 500 mA	1 mA - 2 A, error if I < 1 mA	1 μA - 2.5 A	1 μA - 2.5 A	0.2 - 20/500 mA	0.1 mA - 2.5 A	1 μA - 200 mA	< 10 *T*A - 1 A	variable
Potential input range	+/- 10 V	+/- 10 V	+/- 10 V	+/- 15 V	+/-500 V	+/- 600 V	+/- 500 V	+/- 10 V	+/- 50 V
Max. output voltage	400 V	400 V, 3 kV with booster	400 V, 800 V with booster	400 V, 800 V with booster	160 V, 400 V with booster	250 V	350 V	400 V	400 V
Minimum applicable voltage as source	n/a	4.8 V	2 V	2 V	n/a	n/a	n/a	variable, dep. on current	n/a
50/60Hz noise filtering	analog filter	analog filter	analog filter	analog+digital	analog filter	analog filter	analog filter	software filter	software filter
Operation temperature	-20°C to 70°C	-20°C to 70°C	-20°C to 70°C	-20°C to 70°C	-20°C to 70°C	-20°C to 70°C	-20°C to 70°C	-40°C to +85°C	-40°C to +85°C

$$\rho_{app} \propto \frac{1}{I^2} \tag{2}$$

a...electrode separation, R_{meas}...measured resistance, U_{meas}...measured potential difference, I_{inj}...injected current.
An empirical formula for the penetration depth of measurements using Wenner configuration is given as a/2 (Edwards 1976). For most of the areas within the Alpine region, permafrost thawing processes are expected to happen within the first metres of the subsurface. Therefore, electrode arrays starting with a minimum electrode separation of 20 cm up to a spacing of 4 m were used for the following calculations. Inserting equation 2 into equation 1 considering the used units yields

$$U_{meas}[V] = 0.001 * \frac{I_{inj}[mA] * \rho_{app}[0hmm]}{2 * \pi * a[m]} \tag{3}$$

Consequently, to examine the range of the theoretically expected potential difference, U_{meas} was calculated for electrode distances of 0.2, 0.5, 1, 2 and 4 m (equal to penetration depths of 0.1, 0.25, 0.5, 1 and 2 m) and subsurface resistivities between 500 Ωm and 1 MΩm. I_{inj} was set to 1 mA and 0.01 mA. Figure 2 shows the results of the calculation. It illustrates that for the smallest electrode spacing of 20 cm, only resistivities below 15000 Ωm for 1 mA of injected current can be measured, if the potential input limit of the instrument is just +/– 10 V. Since a much higher resistivity is expected for permafrost areas, lower currents in the range of μA (see Fig. 2) have to be injected or the voltage input range has to be enlarged. However, one microampere is at the edge of the resolution of most current sensors, implemented in several of the commercial systems (Table 2). Moreover, some of the systems, operating with constant current injection, allow only a minimum current value of 0.2–1 mA, which could limit the application in frozen regions.

For most geoelectrical instruments the minimum voltage applied for current injection depends on the voltage of the attached battery (typically between 12 and 24 V), which is in some cases not low enough to produce the required injection currents below 1 mA. Moreover, as Table 2 shows, all instruments, used within the published monitoring case studies, offer an input impedance of just 20 MΩ. Therefore, at high subsurface resistivities during the winter period, a lower measurement resolution and thus, also a higher inversion error has to be accepted. Consequently, we conclude that much attention has to be focused on a proper selection of the survey instrument, depending on the expected subsurface parameters as well as on the evaluation of the reliability of the acquired data.

Hardware adaptations of the Geomon^{4D} geoelectrical system to improve the performance for permafrost monitoring

The Geomon^{4D} automatic geoelectrical monitoring system was originally developed by the Geological Survey of Austria (Supper *et al*. 2003, 2004, 2005) for an optimized monitoring of

landslides (Supper 2007a). Due to the application of innovative electronic components, data acquisition time was reduced, thus allowing the generation of snapshots of the subsurface structure. For a complete subsurface section, usually between 2000 and 4000 data points are measured within less than one hour (for technical specifications see Table 3).

However, the most important improvement is based on the fact that the new system samples each of the measurements several hundred times (usually between 800 and 2000 samples, which gives a total of 2.25 million potential measurements per survey section) and saves all of these single values. A high sampling rate of 0.2 ms is used to detect noise components with higher frequency. At this sampling rate, at least 200 samples are necessary to cancel out the 50 Hz noise component. However, usually at least 800 samples are taken to make averaging more accurate.

The large amount of single samples for each data point allows for the possibility of applying enhanced noise analysis algorithms and performing an adapted data quality evaluation, directly involving the raw data time series values and not just averages. This innovative process ensures that only those (averaged) data points with the highest quality are used for subsequent data inversion.

Additionally, several options for remote access and data transfer were implemented to the system: measuring results are sent automatically by email each day and system maintenance and data download can be remote-controlled. The results of several test measurements (Supper *et al*. 2010) showed that for long term permafrost monitoring, further adaptations had to be applied to the Geomon^{4D} system to improve its performance.

As mentioned in the chapter 'Implications for permafrost monitoring', severe problems could arise from the fact that the contact resistivity at the electrode-ice border might change during the measuring cycle when injecting currents. This behavior has been indicated by several test surveys. In order to eliminate this effect, two major measures were taken. First, electrodes for current injection and potential measurements were separated. Only every fourth electrode was dedicated for current injection, and the three electrodes in between for potential measurement. This also minimizes possible polarization effects. However, since the gradient configuration was used as a measuring sequence, sufficient coverage can easily be reached. Second, a feedback regulation algorithm was implemented for the current source, which allows current to be stabilized even during the phase of injection in case of changing contact resistivities. Additionally, the developed constant current source was adopted to allow the application of voltages below 12 V to fit the measured signal at very high resistivities to the required input voltage range of +/– 10 V. This requirement was especially pertinent to measurements taken during the thawing period. When thawing starts within the surface layer, very low contact resistivities allow the injection of comparably high currents while subsurface resistivities at shallow depths are still very high. Consequently, even at applied voltages below 12 V the measured potential differences still exceed the input range of several systems (Table 2).

Since permafrost monitoring is usually carried out at very remote and exposed locations, a special module had to be developed for lightning protection, which protects every single input and output channel against overvoltage. Additionally, as access to the installation site of the system would be almost impossible during winter time, a power supply by a fuel cell was implemented and tested, allowing a permanent operation without the need to refuel for more than 8 months. An additional solar power supply was not foreseen due to the danger of lightning strikes. To

TABLE 3
Technical specifications of the GEOMON^{4D} system.

GEOMON^{4D} specifications	
sampling rate	0.2 ms
delay between current on an potential sampling	20 ms
delay between forward and backward current injection	120 ms
duration of current injection	160 ms
average time to measure one data point including gain ranging	0.8 s
average number of samples for permafrost monitoring	800
number of data points/section	2601
average deleted data points	200

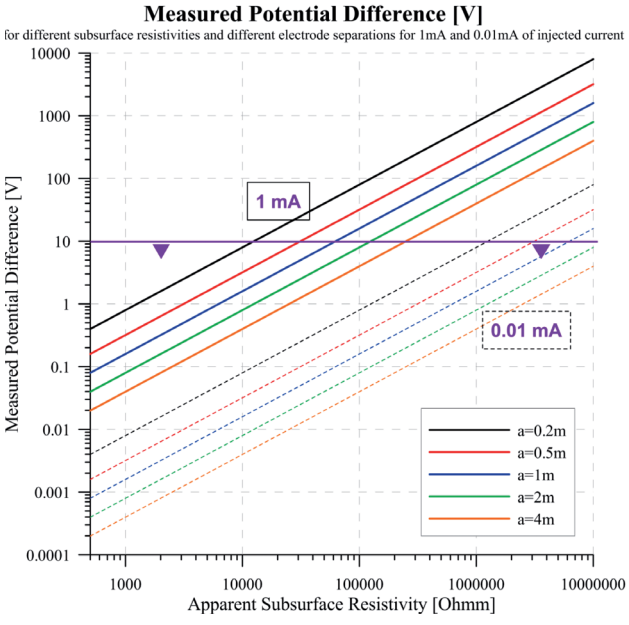

FIGURE 2
Calculated relation between subsurface resistivity and measured potential difference for an injection current of 1 mA and 0.01 mA.

save power, only one measurement of a full section per day as well as an automatic shut down after the measurement was foreseen. The geoelectrical equipment, fuel cell and batteries were placed in casings especially developed for harsh conditions (see Figs 8 and 14). The exhaust heat from the fuel cell was also used to prevent the geoelectrical system from freezing.

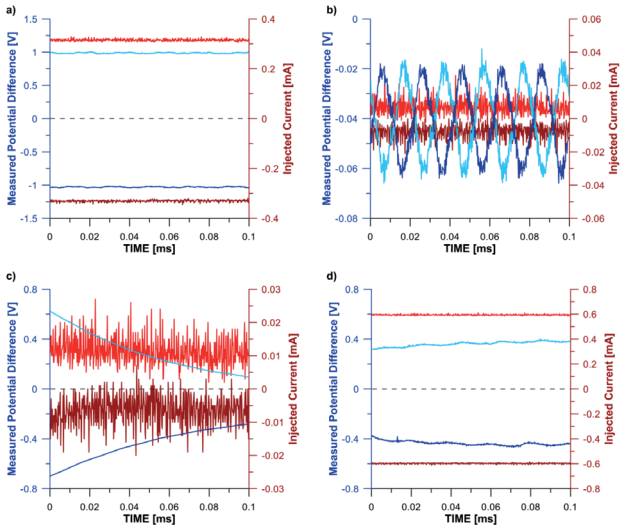

FIGURE 3

Typical categories of raw signals measured at the Magnetköpfl/Kitzsteinhorn site; light blue: measured forward potential difference; dark blue: measured backward potential difference; light red: forward current; dark red: backward current.

Data quality assessment algorithms to assure the generation of optimized data sets for data inversion

The special capability of the Geomon^{4D} system, i.e. to save all single samples of raw measurements, was used to develop an automatic analysis tool to thoroughly check and analyse the data quality of each measurement. A careful analysis of several thousands of raw samples from field measurements in different geological environments showed that mainly four typical categories of sample shapes exist. Figure 3 illustrates typical examples for these four major categories of raw signals. The top left picture (a) displays a measurement with a very good signal-to-noise ratio, whereas in the top right picture (b) a measurement done at a low injection current is displayed. Due to the high levels of background noise (mainly 50 Hz and multiples) hardly any differences between forward and backward potentials can be derived. The bottom left graph (c) shows again a measurement performed with a very low injection current. Potential differences in this case contain a smooth drift, whereas no 50 Hz (+ multiples) noise component is detectable in the recorded potential signal. This case is typical for non- or badly connected electrodes. Finally, the bottom right chart (d) presents a measurement with a sufficiently strong current injection, whereas potentials show significant drifts which could be due to polarization effects or long periodic background noise.

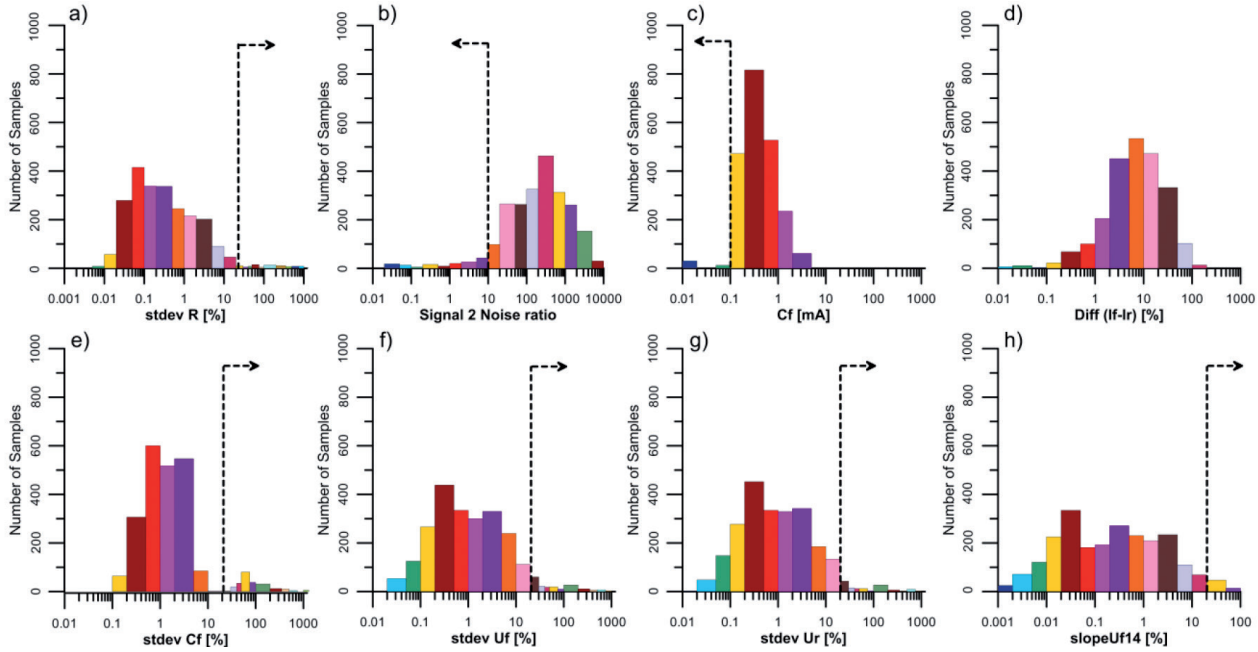

FIGURE 4

Results of statistical analysis of a typical measurement; a) standard deviation of apparent resistivity for two different intervals of the raw data time series; b) Signal to noise ratio; c) injection current forward; d) difference between injection current forward and backward; e) f) g) standard deviation for two different intervals of the raw data time series of injection current forward, potential difference forward and potential difference backward respectively; h) Slope of the potential difference forward between two different intervals (1 and 4) of raw data time series; black dashed lines with arrows indicate the filter thresholds.

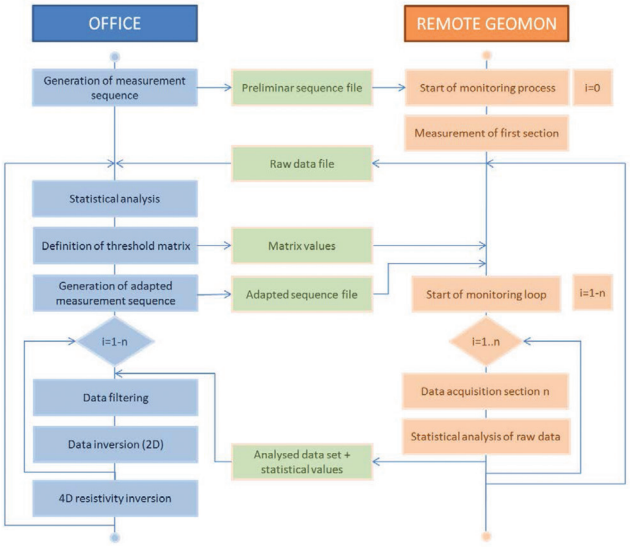

FIGURE 5
Data acquisition and processing workflow for the GEOMON^{4D} system; variable n is usually set to 15 or 30 days.

Based on these findings, the following criteria were used to evaluate the quality of the measurements (Fig. 4 shows the analysis results from a typical measurement):

1. Injection of a constant current should be possible at an adequate level (Fig. 3a). To analyse this, distributions of absolute current values within the whole data set as well as their standard deviations are calculated and cut off values are defined (Fig. 4c, e).
2. Potential differences measured for forward/reverse current injection should show clearly distinguishable levels, significantly above noise level (see Fig. 3b as negative example), and no drifts. Consequently, for each measurement, standard deviations of the potential (forward and backward; Fig. 4f, g), a measure for noise content as well as signal-to-noise ratios (Fig. 4b), defined by formula (4) are calculated:

$$SN = \frac{\left| |U_{fM}| - U_{rM} \right|}{\frac{1}{2n} * \left(\sqrt{\sum_{i-1}^{n} \left(U_{fi} - U_{fM} \right)^2} + \sqrt{\sum_{i=1}^{n} \left(U_{ri} - U_{rM} \right)^2} \right)} \quad (4)$$

$$U_{fM} = \frac{\sum_{i=1}^{n} U_{fi}}{n} \quad (5)$$

$$U_{rM} = \frac{\sum_{i=1}^{n} U_{ri}}{n} \quad (6)$$

U_f…Potential difference for forward current injection
U_r…Potential difference for reversed current injection

To determine a measure of repeatability, the raw data time series are sub-divided into four intervals. In each of the intervals, the average apparent resistivity as well as the standard deviation of these values (Fig. 4a) are calculated.

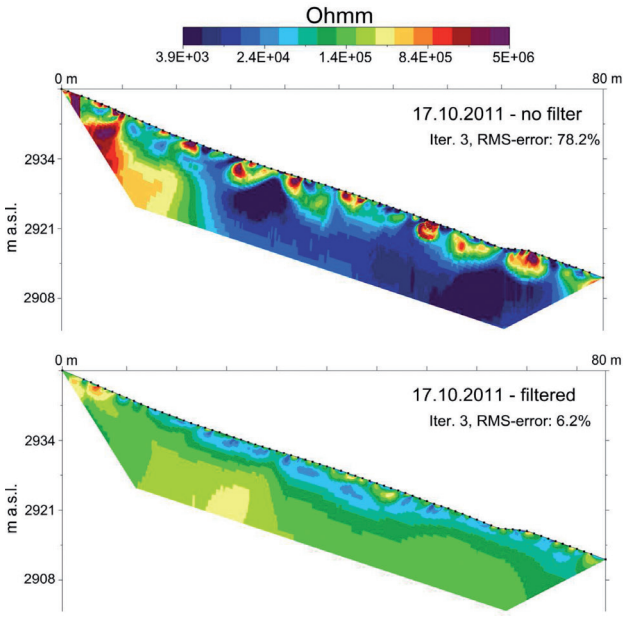

FIGURE 6
Inversion results of the raw data set (no filter) and of the filtered data set.

For each single data point of a section the values defined above are calculated.

Based on the statistical distribution of these values of the whole data set (Fig. 4), thresholds are defined by manually evaluating the different statistical distributions. They are summarized in a threshold matrix. This matrix is then used for filtering all raw data sets for a certain period before data inversion. Since the raw data set comprises a large amount of data, which cannot easily be sent by UMTS connection, the statistical analysis of raw data sets is performed on the remote monitoring system and only the averaged data points and the results of the statistical analysis are sent by email each day. Experience showed that the threshold matrix is in general site dependent and can be used for a period of several months. However, raw data sets are also downloaded every two weeks to check the performance of the filtering (see Fig. 5 for details on the workflow).

Figure 4 gives an example of the results of such a statistical analysis. Black lines and arrows indicate the determined threshold values used for data inversion. Figure 6 compares the inversion results of an unfiltered raw data set (from the Kitzsteinhorn site) with the results of the filtered version. Although rather tolerant thresholds were set, a significant improvement in the inversion error from 78 % to 6 % can be recognized.

In general, the improvement in data quality turned out to be seasonal dependent. For example at the Kitzsteinhorn site we had to delete around 300 data points in autumn to come down from around 70% to 6% of inversion error, whereas in winter around 800 points had to be discarded to reduce the error from 80 to 20% and during summer only 80–150 to reduce the error from 15 to 4%.

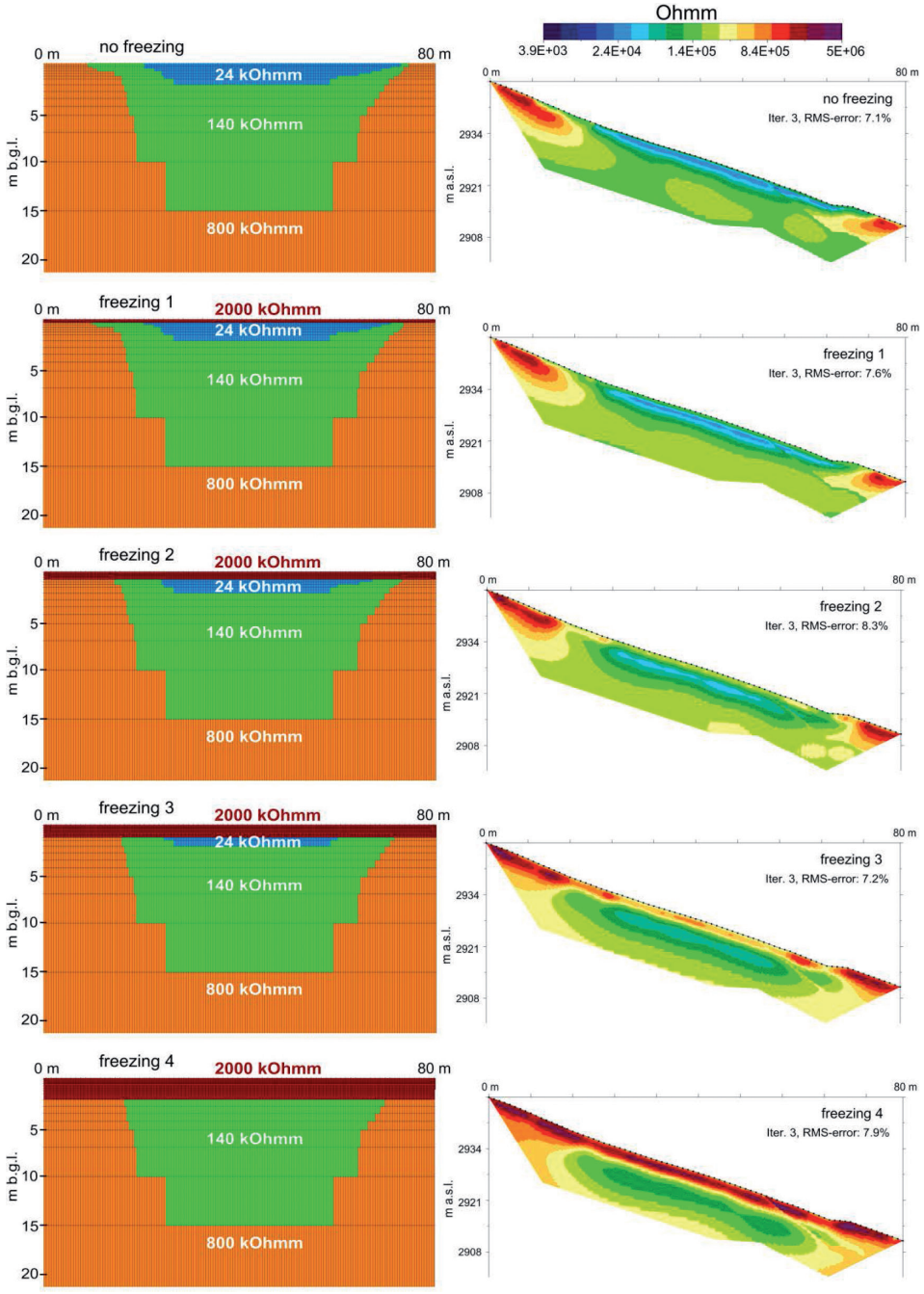

FIGURE 7
Modelling of the freezing process and the influence on the inversion result.

These results highlight the necessity of introducing an automated data quality assessment and filtering procedure into the raw data processing workflow. In several cases, for example during the whole winter period (phase 3) for the Kitzsteinhorn site, meaningful inversion results could only be derived when applying a strict selection, based on such criteria. It has to be pointed out that such a selection is only possible if the instrumentation used for monitoring allows the saving of raw sample data. Consequently, in our point of view, this is a precondition to assessing data quality and to producing high quality results.

Data inversion

Several authors (e.g., Hilbich *et al*. 2009, Krautblatter *et al*. 2010) have already reported in detail about problems related to the inversion of data at high resistivity contrast. Difficulties arise on one hand from the inherent, general ambiguity of geoelectrical data inversion, which is manifested in a tendency of commercially available software codes to smooth out resistivity contrasts. Figure 7 illustrates this effect using forward modelling and successive inversion of the modelled data set, simulating the special resistivity structure at the Kitzsteinhorn test site.

Although only the resistivity of the surface layer is assumed to change its value (simulating freezing of the active layer from the surface), the inversion results also show significant resistivity variations at larger depths. On the contrary, the results prove that freezing processes close to the surface can be mapped quite accurately, which confirms the field results from Hilbich *et al*. (2011).

On the other hand, since the measurement of high resistivities at such low currents is at the edge of what current data acquisition and processing technology can achieve, noise and measuring inaccuracies (e.g. those originating from leakage currents of the amplifier and low input impedances) might result in inversion artifacts. Therefore, in our point of view, a careful assessment of raw data quality, as described above, is a prerequisite to high quality inversion results.

For data inversion results shown in this paper, the AGI EarthImager™ code was used. Other inversion codes (i.e., Loke *et al*. 2003; Kim *et al*. 2009), which go beyond the standard smoothness-constrained inversion, were also tested, but they did not lead to significantly better results.

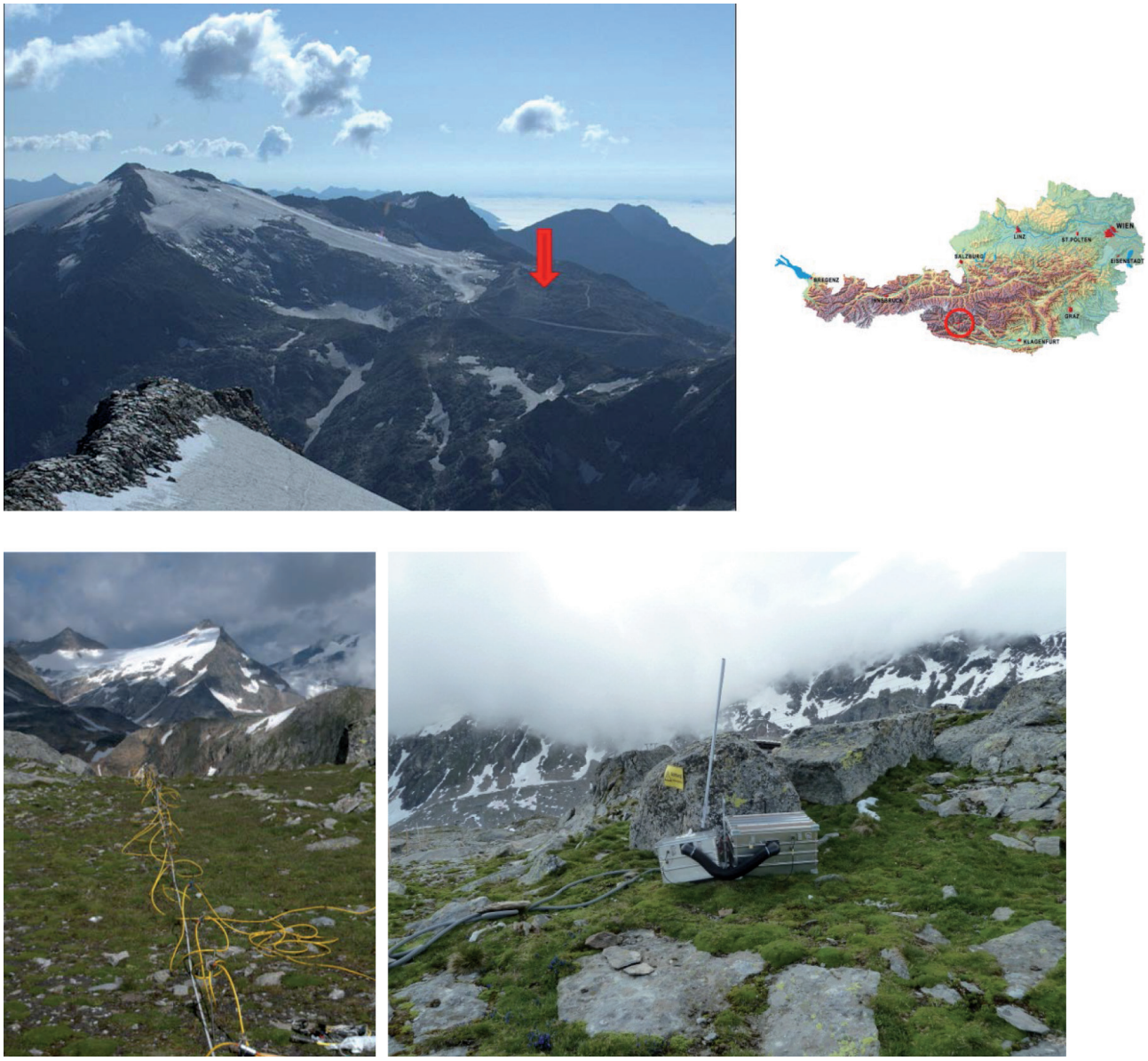

FIGURE 8

Location of the geoelectrical monitoring profile close to the cable car station Eisseehaus at the base of the Mölltaler Glacier (top left); location of the test site within Austria (top right); view on the monitoring line towards "Hoher Sonnblick" in the back; casing of the Geomon^{4D} and of the fuel cell.

RESULTS FROM PERMAFROST MONITORING FIELD TEST SITES

The geoelectrical monitoring installation close to the Mölltaler Glacier

Due to its good accessibility even during winter time, an area close to the "Eisseehaus" at the Mölltaler Glacier in the Austrian Alps was selected for the first permanent monitoring installation (Fig. 8). The subsurface at the location of the monitoring profile consists of granite and gneiss partly covered by a thin layer of weathered material. At the end of September 2010, a profile consisting of 81 stainless-steel electrodes, positioned at an equal spacing of one metre, was installed at an altitude of around 2770 m. The adopted Geomon^{4D} system, as described before, was used as a measuring device and a SFC Efoy Pro© 600 fuel cell with two methanol tanks as a power supply. Data transfer was implemented using a commercially available USB internet stick from a local mobile telephone company. From October 2010 until mid-July 2011, one complete data set consisting of 2590 single measurements distributed in a gradient array, was measured once a day. The fuel cell had to be refuelled only once in May after 8 months of permanent operation.

Analysis of temperature data

Since no soil temperature data were available for the Mölltal Glacier area, temperature data measured in boreholes close to the Sonnblick observatory (4.5 km distance, but at a higher altitude around 3100 m) were used for interpretation (Fig. 9 and Fig. 10). Since subsurface geology, slope orientation and snow cover is comparable we could assume that the general temperature trend will be similar and only a minor temperature shift can be expected. To validate this, we compared air temperature measurements at Sonnblick (3111 m) with air temperature measurements at Fraganter Scharte (2743 m, 800 m distance from the monitoring site). The results verified that most of the temperature events happen at the same time. Moreover averaged air temperature values showed only differences of 1.5–2°C in winter time, 1.5°C during the spring period and around 1°C during the summer period on an average between the two stations. A comparison of soil and air temperature data from Sonnblick also showed that average air temperature values have to be damped by approximately 50% (respecting a phase shift) to calculate estimated soil temperature values similar to the ones measured at Sonnblick. Consequently, based on these data and calculations, we conclude that we do expect higher soil temperature values at our monitoring site at Mölltaler Glacier compared to the available data from Sonnblick, but only in the range of +0.75 to +1°C. Consequently all plotted values were adjusted by +0.75°C.

Borehole temperature values (Fig. 9 and Fig. 10) at 0.8 m depth clearly show several distinct phases: a period with almost constant values around zero degrees (phase 1) lasted until mid-

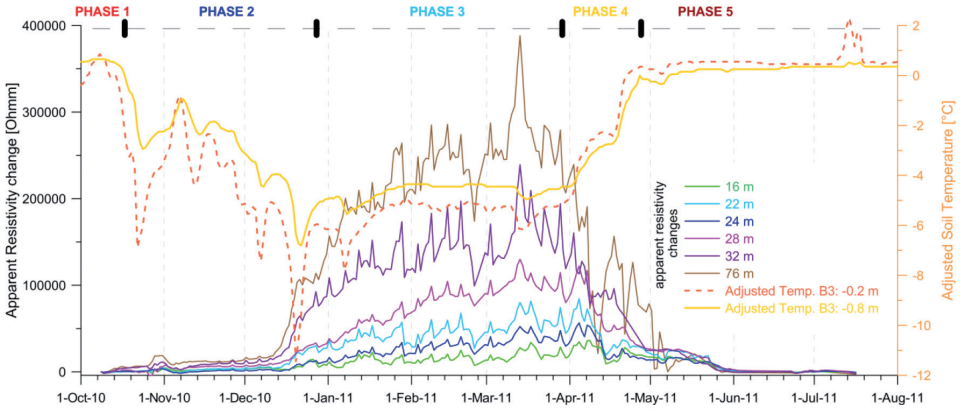

FIGURE 9
Comparison between apparent resistivity change for an apparent depth of 1 m at different locations along the profile and adjusted soil temperature for two depths (0.2 m orange dashed line and 0.8 m yellow solid line, soil temperature data originate from borehole at "Hoher Sonnblick").

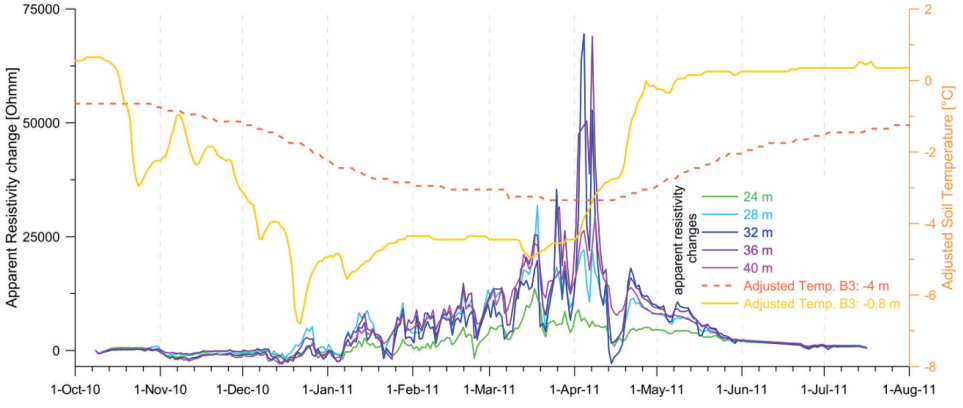

FIGURE 10
Comparison between apparent resistivity change for an apparent depth of 4 m at different locations along the profile and adjusted soil temperature for two depths (4 m orange dashed line and 0.8 m yellow solid line, soil temperature data originate from borehole at "Hoher Sonnblick").

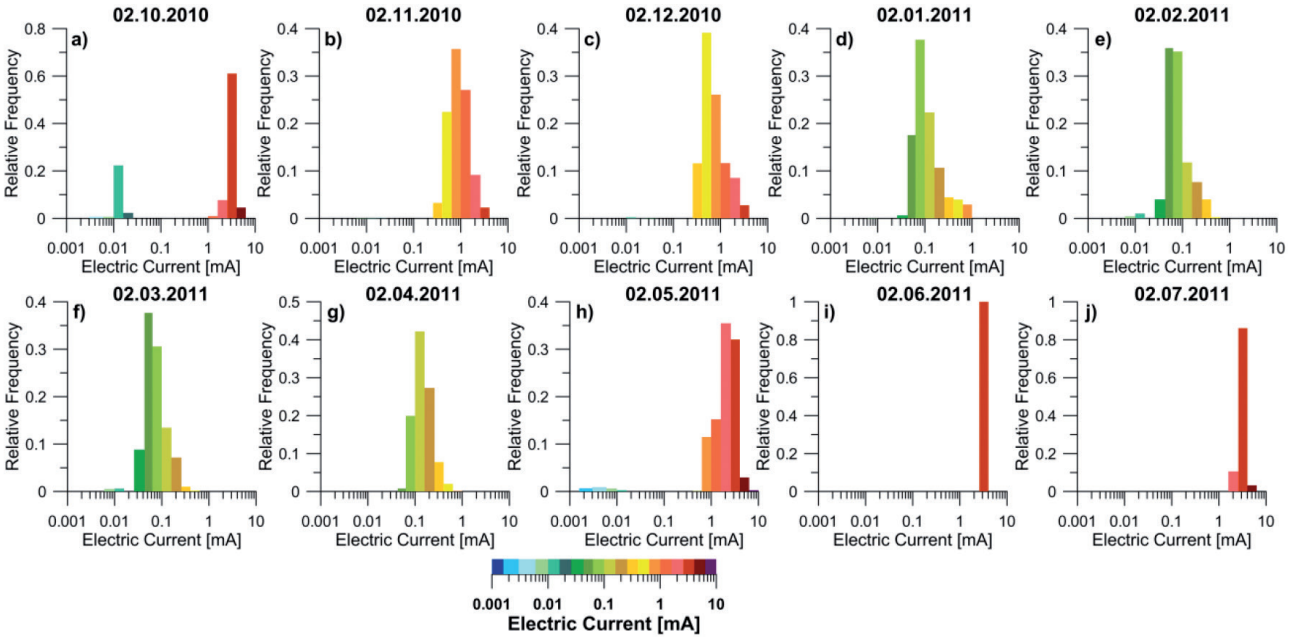

FIGURE 11

Statistical distribution of injected currents at different times for the monitoring profile Mölltaler Glacier, colours indicate ranges of current.

October, when a sudden temperature drop was followed by a time with slowly decaying values, lasting until the end of November (phase 2). At the end of phase 2, surface temperatures dropped suddenly below –11°, thus inducing a sudden decrease of temperature also at 0.8 m depth with a certain delay. This event marks the transition to phase 3 (winter period), characterised by a very constant temperature (average –4.5°C at a depth of 0.8 m), which lasted until the beginning of April, when it was followed by a sudden rise of temperature (phase 4 till end of April). Afterwards, temperatures smoothly rose again, marking the period of successive thawing of the subsurface (phase 5).

Analysis of current distributions

Figure 11 shows the statistical distribution of injected currents for different times. During the first days of measurement, most of the injected currents were found between 2 and 6 mA (in fact the maximum range allowed by the system). Some days after the installation, when surface soil temperatures dropped significantly below zero degrees, most of the injection currents were detected in the range between 0.5 and 2 mA, whereas after another major temperature drop in mid-December, mainly currents in the range between 0.05 and 0.3 mA could be injected. Values remained in that low range until the end of April, when most registered currents were again above 1 mA.

Analysis of apparent resistivity time series

Figure 9 and Fig. 10 also display the change of apparent resistivity for selected configurations, positioned at successive locations along the profile (profile distance 16, 22, 24, 28, 32 and 76 m), for an approximate penetration depth of 1 and 4 metres, respectively. The different characteristic temperature phases are also reflected in the changes of apparent resistivity. Apparent resistivity stayed at a very constant and relatively low value until the first drop in temperature, after which apparent resistivity began to rise continuously.The sharp temperature drop at the beginning of December initiated a strong rise of the apparent resistivity. The following phase is characterised by rapidly changing values, which lasted until nearly the middle of April. It is conspicuous that all apparent resistivity curves follow the same trend, which might indicate a relation with surface conditions (e.g., electrode – soil contact, change of surface layer (first 5–10 cm)).

With a delay of more than two weeks compared to the temperature trend, apparent resistivity values reached the original low values again at the end of May.

The five phases can be interpreted in the following way: During phase 1, only freezing of the surface layer with periodical thawing took place. The electrodes penetrated the frozen layer. Variations in apparent resistivity are small. In phase 2, freezing of the surface layer proceeded and apparent resistivity changes are mainly caused by a reduction of porosity due to an increased fraction of frozen water. A significant amount of fluid water is still present within connected channels. In the third phase, apparent resistivity suddenly increases rapidly. We assume that in this phase, almost all brine channels are disconnected. Only a very small and probably very variable amount seems to be still connected. The background conductivity most probably can be attributed to surface charge mobility. Injection currents during this phase were also very low, thus the error in determining values for apparent resistivity is also very high. A comparison of Fig. 9 and Fig. 10 shows that for shallow depths, apparent resis-

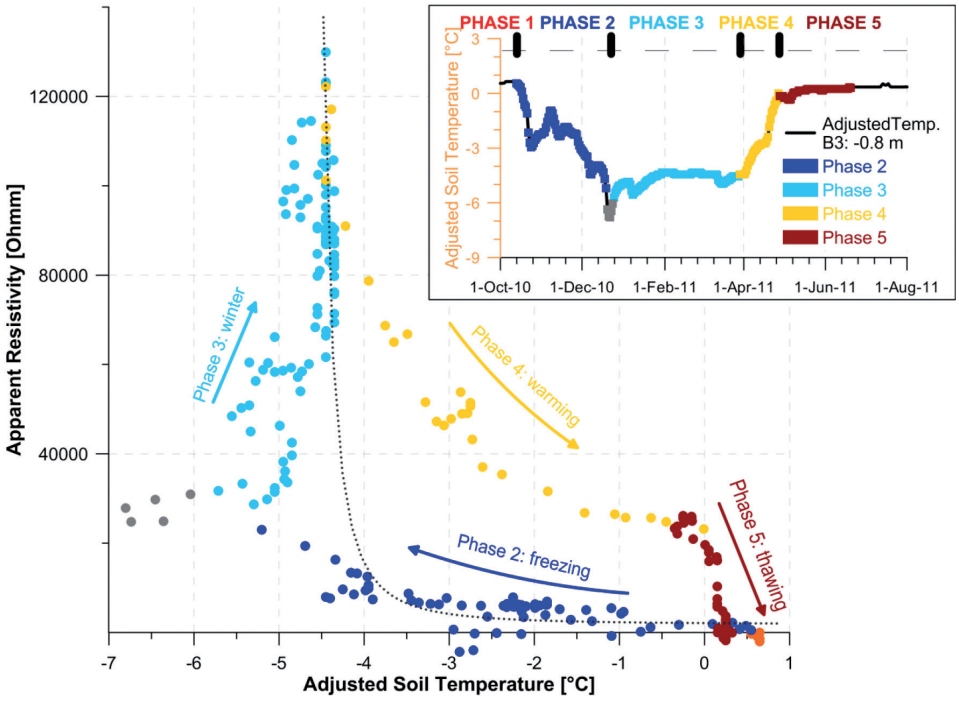

FIGURE 12
Relation between adjusted soil temperature (soil temperature measured at "Hoher Sonnblick" – approx. 5 km distance, see also comments in text) and apparent resistivity (apparent depth 0.8 m, mid of profile) at Mölltaler Glacier with the indication of different phases; data from different phases plotted on the time series of adjusted soil temperature (top right).

tivity values vary quite a lot along the profile, whereas values at depth exhibit a very similar behaviour along the profile. This might be due to the different slope angles along the left (northwestward orientation) and right (almost horizontal) part of the profile. However, since no data is available on different snow coverage along the profile, further interpretations would be only speculative.

Analysis of the dependency between resistivity and temperature

Figure 12, showing the dependency between apparent resistivity and soil temperature, also highlights the different characteristics of each phase: Phase 1, in which the temperature varies around 0°C, is not well resolved due to a lack of resistivity data. In phase 2 (dark blue) the soil temperature successively drops from 0.5°C to –5°C. The dependency between apparent resistivity and temperature seems to be non linear, especially for temperatures below –4°C. The dependency in phase 3 cannot be determined, since the variations of apparent resistivity values are very large compared to the variations in temperature (max. 1°C). Since temperatures are not measured at the same place, uncertainties are too high for an exact interpretation. Consequently, assuming an uncertainty in the temperature data for deeper temperatures, phase 2 and 3 could also be combined (dashed curve), resulting in a non-linear dependency curve of Φ^{-m} – shape (similar to Archie's law). This suggests that in these phases resistivity is mainly determined by a decrease in porosity caused by a successive shrinking of brine channels. Values during phase 4 again clearly exhibit a non-linear dependency, most probably characterising an increase of porosity due to the successive development of connected brine channels. Above 0°C the relation is simply linear. This suggests that in phase 5, apparent resistivity is mainly determined by temperature variations (linear relationship). At the end of the observation period, values reach almost the same level as in autumn the year before. It seems that the curve of temperature dependency of the apparent resistivity follows a hysteresis like curve, whose shape might be used to characterise the active layer of a certain area. A hysteresis like behaviour was already reported by Lukin *et al*. (2008), Murrmann (1973), Grimm *et al*. (2008) and Krautblatter *et al*. (2010) and could perhaps be contributed to the supercooling of the pore fluid (Lukin et al. 2008) instead of freezing point depression. To investigate these dependencies quantitatively in more detail, long time observations as well as soil temperature measurements on the same profile are necessary. It is interesting to note that the change in the temperature-resistivity dependency happened at almost the same temperature (–0.2°C) as was reported by Krautblatter *et al*. (2010). However, in the Zugspitze test study temperatures were not low enough to recognize a possible non-linear dependency.

Resistivity inversion results

The inversion results (Fig. 13) show a successive penetration of the freezing front, initiated by mid-December, until the beginning of April, when the thickness of the frozen surface layer started to decrease again. The higher inversion error during winter time is most probably due to much lower injection currents (Fig. 11), associated with a larger noise component and a lower measurement accuracy. However, inversion results also showed that resistivity values for depths larger than 5 m

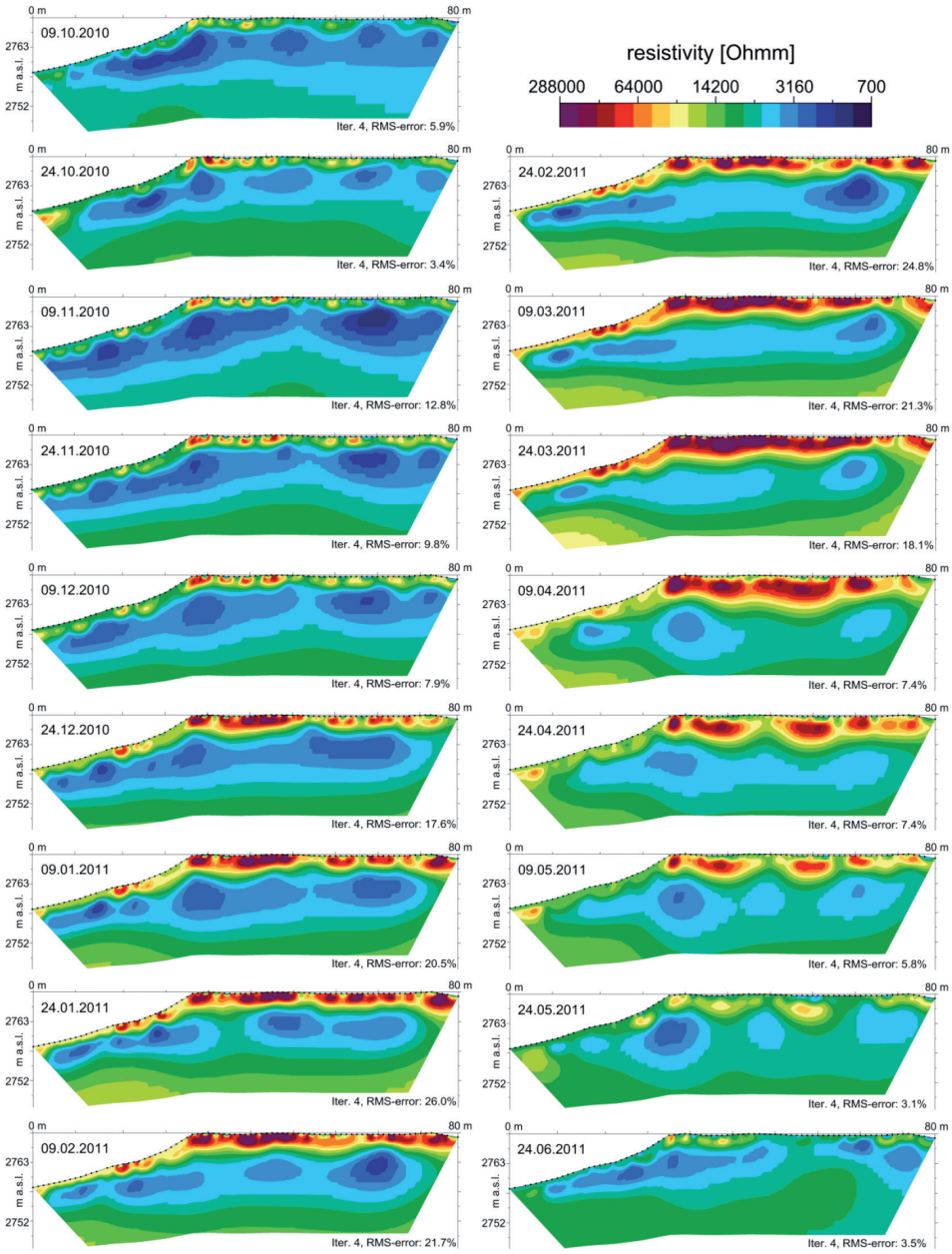

FIGURE 13
Selected inversion results covering the monitoring period from October 2010 to June 2011 measured at the monitoring site Mölltaler Glacier.

remained at low values (between 1000 and 5000 Ωm) during the whole winter period. Only in spring was a small but general increase of resistivity at medium depth detected due to the usual delay of the temperature minimum for larger depths and/or the infiltration of highly resistive snow melt water. This is also verified by Fig. 10, showing apparent resistivity time series from configurations with a higher apparent penetration depth. The absolute values are much smaller than for an apparent depth of 1m (Fig. 9), and their maximum is shifted towards springtime. Therefore, we can conclude that at this test site no permafrost is present. Consequently, a topographically higher location was chosen as a test site for the following seasonal cycle.

Geoelectrical monitoring at the Magnetköpfl/Kitzsteinhorn site

In October 2011 the monitoring system was removed from Mölltaler Glacier and reinstalled on the north facing ridge of the Magnetköpfl close to the Kitzsteinhorn peak at an altitude of approximately 2920 m a.s.l. (for location see Fig. 14). At this location increasing rock instability due to the disappearance of permafrost as well as the decrease of glacier height followed by a lack of counter pressure onto the flanks of the slope had already been observed (Hartmeyer *et al*. 2012). To support the interpretation of geoelectrical monitoring data, four temperature sensors were installed at two locations at two different depths (10 and 80 cm b.g.l.) directly on the profile (one location shown in Fig. 14e, Keuschnig *et al.* 2012).

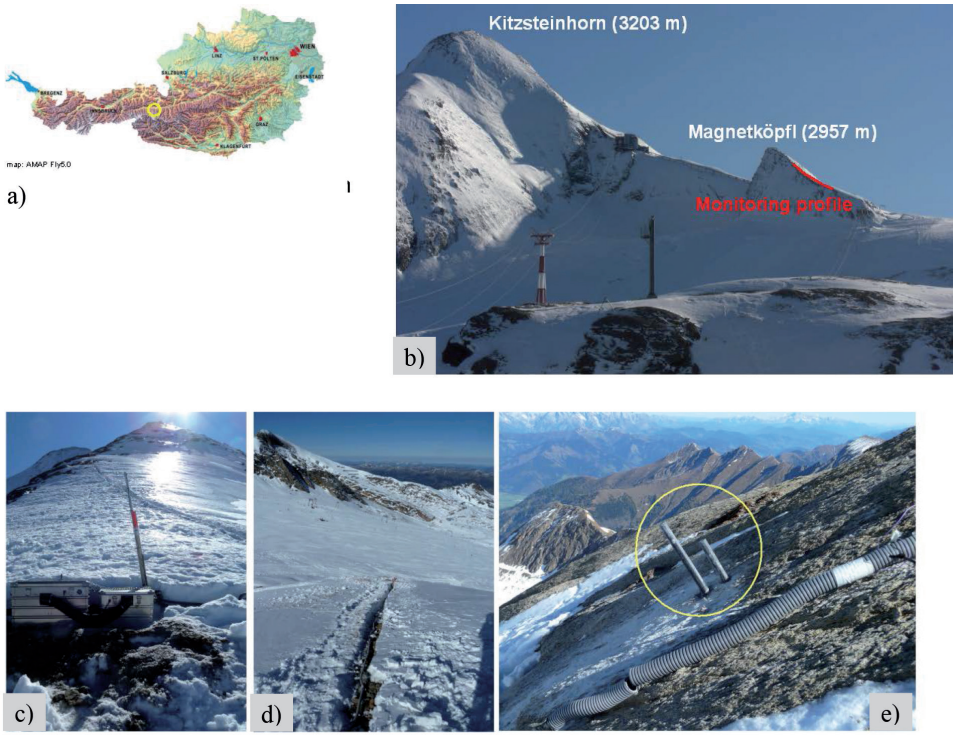

FIGURE 14
Location of the monitoring site Magnetköpfl/Kitzsteinhorn; a) location of the site within Austria; b) view of the summit area of the Kitzsteinhorn with the indication 39 of the monitoring profile; c), d) view on the monitoring location; e) location of the soil temperature sensors.

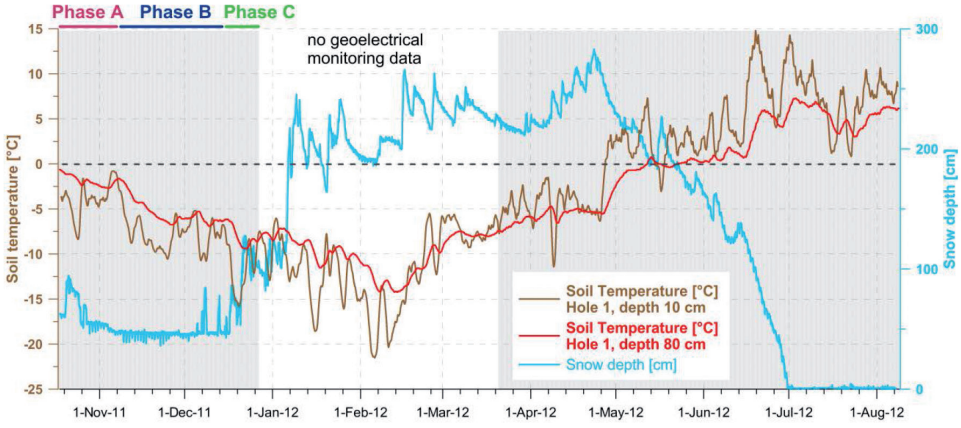

FIGURE 15
Results of soil temperature at two different depths (red and brown line) and snow depth (snow depth data was collected approximately 200 m to the monitoring location).

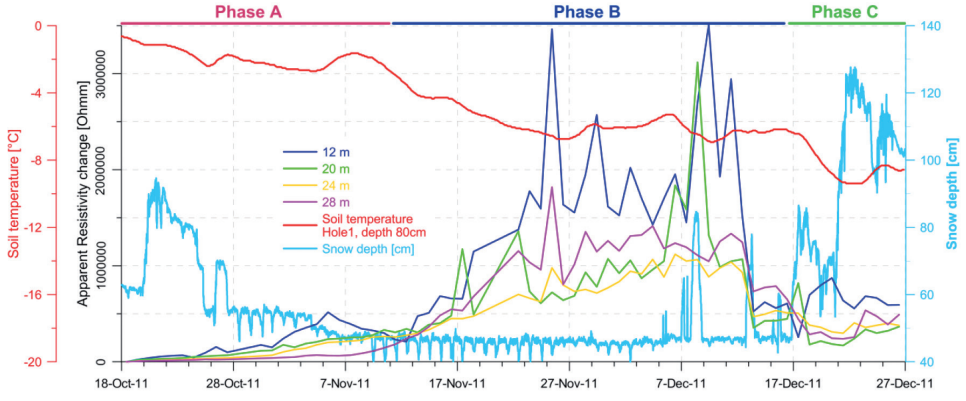

FIGURE 16
Comparison between apparent resistivity change (differences to the first measurement in October) for an apparent depth of 1.5 m at different locations along the profile and soil temperature at a depth of 0.8 m monitored at the Magnetköpfl/Kitzsteinhorn site for the period October 2011 to December 2011 (snow depth data was collected approximately 200 m to the monitoring location).

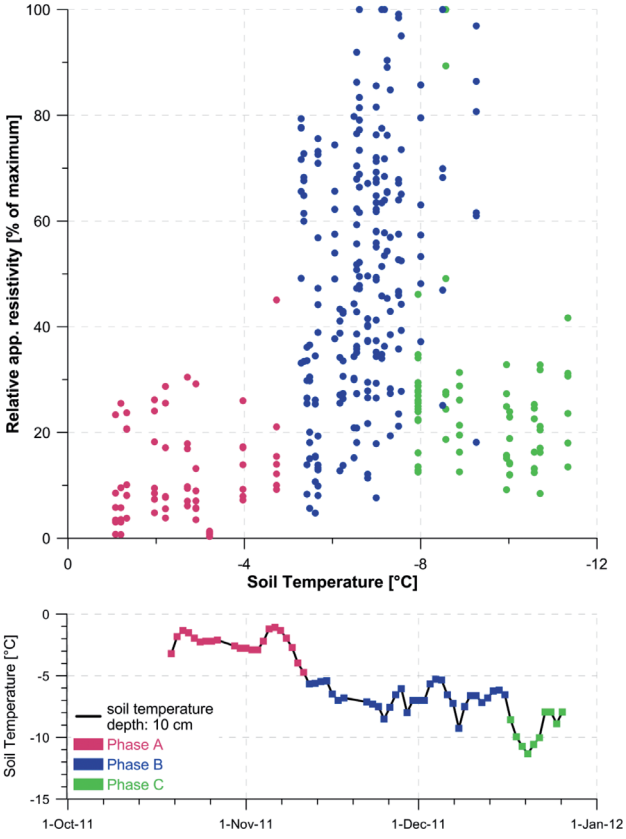

FIGURE 17
Relation between soil temperature and relative apparent resistivity where different colours indicate different phases; data from different phases plotted on the time series of soil temperature (bottom).

On December 27th the power supply of the system failed. Due to the remote location of the installation, the system could not be accessed until mid-March. In the period between March and June, the system partly failed because of a bad cable connection on one transmitter board. Hence, only selective time series of apparent resistivity and no inversion results are available for this period.

Analysis of temperature data

Figure 15 shows the results of the soil temperature measurements, taken at hole1 at profile distance 5.5 m, and of snow depths, which were measured in the nearby ski area. Due to the wind exposed location of the monitoring site, snow depth can be assumed to be lower at the monitoring profile than in the ski area. Therefore for interpretation purposes, we only refer to the times of snow events. In general, the soil temperature time series at 10 and 80 cm depths show a successive decrease till the beginning of February, when the lowest temperature of –15°C was reached in 0.8 m depth. After February 15th, temperatures started to rise again with three periods of increased gradient, i.e. mid to end of February, end of April and mid-June. The most prominent temperature rise took place at the end of April, when temperatures increased from –5°C to almost 0°C within 14 days at 0.8 m depth.

Focusing on the period between the start of the survey and the breakdown of the fuel cell in detail, three different phases can be recognised: at first, a period with almost constant (sensor at 10 cm) or smoothly decreasing (sensor at 80 cm) temperature is apparent (phase A), followed by a sudden decrease after November 8th till the end of November, after which temperature slightly rose again and stayed almost constant till December 17th (phase B). At this date, temperatures started to decrease again (phase C).

Analysis of apparent resistivity time series

Figure 16 shows selected apparent resistivity values for a pseudo depth of 1.5 m for different locations along the profile. Until December 13th, the apparent resistivity trend correlates well with the changes in soil temperature: a decreasing temperature trend goes hand in hand with an increase in apparent resistivity. Until the beginning of November, apparent resistivity increased very smoothly (phase A). After the sudden temperature decrease at the end of phase A, apparent resistivity rose significantly up to more than 1 MΩm. During phase B, characterised by almost constant average soil temperatures, apparent resistivity on average remained very high, but its absolute values changed rapidly. Finally, after December 13th at the beginning of phase C apparent resistivity suddenly decreased again, although a further temperature decline took place after December 17th, which was not reflected in any obvious change of apparent resistivity.

Analysis of the dependency between resistivity and temperature

Figure 17 shows a correlation of apparent resistivity values and soil temperature for selected configurations. The different phases are indicated with different colours (phase A: red, phase B: blue, phase C: green). This plot clearly shows that in the range of temperatures between –5°C and –7°C, values of apparent resistivity vary a lot, whereas above and below this range very consistent values could be detected.

Analysis of data quality

For data quality assessment, the distribution of currents and the measured voltage was analysed. Figure 18 displays the statistical distribution of injected currents. At the beginning of the monitoring period (phase A) currents between 0.03 and 1 mA were injected (Fig. 18a–e). Soon after, the median value was shifted successively towards lower values (Fig. 18f, current range: 0.01–0.1 mA), until in phase B only very small currents between 0.001 and 0.1 mA (median value around 0.01 mA, Fig. 18g–h) were injected. In phase C, the injected currents were once again shifted to the 0.01 to 0.1 range (Fig. 18i). In June 2012, without exception all injected currents were in the range between 1 and 2 mA (Fig. 18j). A comparison with Fig. 11 shows that at this site much lower currents could be injected during winter time, which is due to the different geological settings of the surface layers (mostly hard rock at Kitzsteinhorn and residual soil at Mölltaler glacier). As mentioned above, only incomplete data coverage is

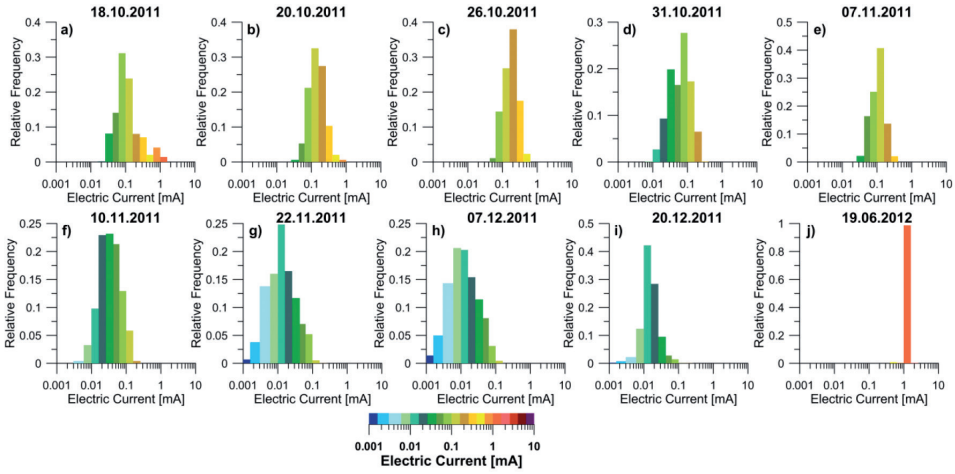

FIGURE 18
Statistical distribution of injected currents at different times for the monitoring profile Magnetköpfl/Kitzsteinhorn, colours indicate ranges of current.

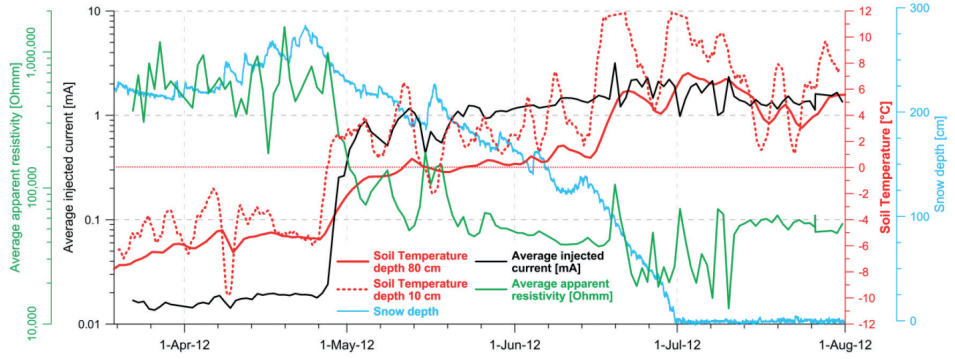

FIGURE 19
Comparison between soil temperature, snow depth (snow depth data was collected approximately 200 m to the monitoring location), average injected current and average apparent resistivity for the monitoring period from March to August 2012 at the Magnetköpfl/Kitzsteinhorn site.

available during springtime. However, to qualitatively evaluate results, average values of injected current and resistivity of available configurations were calculated (Fig. 19). The results clearly show that the major thawing phase was confined to a period of just three days at the end of April. It is well indicated by a rise in temperature as well as an intense rise of average injected currents and a decline of resistivity. Snow depth shows no distinct correlation to the other displayed parameters.

Measurements of the background noise potential detected a strong 50 Hz noise component of approximately 15 mV for an electrode separation of 1 m, most probably due to the different infrastructural facilities (cable cars, ski lifts, etc.) of the nearby ski area. For that reason the distribution of the sum of absolute values of forward and backward voltage was evaluated, which is a measure of the signal to noise ratio. The results definitely exhibit very similar distributions for all phases, with values significantly above the noise level. Therefore we can conclude that even during the period of very low injection currents a voltage signal with a good signal to noise ratio could be detected.

Resistivity inversion results

All data values were carefully checked on sufficiently high signal to noise ratio before inversion. Figure 20 shows the results for data sets at selected times of the autumn to winter period. In the beginning, relatively low values of resistivity are still apparent close to the surface. Successively, more and more high resistivity areas develop within the shallow subsurface, and resistivity at larger depths also slowly decreases (phase A). In phase B, the thickness of the highly resistive surface layer has increased, whereas the resistivity at depth stays almost constant but at a higher level than until November 18th. After December 13th (phase C), the thickness of the surface layer has decreased again, especially in the middle part of the profile. The inverted sections for the spring and summer period (Fig. 21) show a relatively low resistive surface layer (partly thawed surface), whose thickness is increasing with time, and also resistivities at depth are successively increasing. Finally, in September, almost the same resistivity pattern is reached as when monitoring began in October 2011. To investigate the significance of resistivity changes at larger depths, forward modelling (Fig. 7), assuming a successive freezing and thawing of the surface layer for this special site condition, was performed. The results proved that resistivity changes at larger depths can be due to inversion errors and that the results at this site could be fully explained by a simple surface freezing process.

DISCUSSIONS

Within recent years research has focused on improving the data acquisition technology for geoelectrical monitoring of perma-

frost related phenomena. Several field tests proved that it is possible to yield reliable potential difference measurements when injecting low currents into frozen ground, even at soil temperatures below –10°C. However, to derive reliable data much attention has to be paid to the quality of the measuring technology as well as to a comprehensive data quality assessment. First of all, since very low currents have to be injected to measure the high resistivities expected in such environments (100–1000 kΩm), very sensitive current sensors are needed, which should allow the measurement of currents in the range of +/– 1 μA where the surface layer is frozen. The study at hand further shows that inversion results would significantly improve when full raw data samples and not only arithmetic averages of these values are recorded and analysed. This ensures that only reliable high quality measurements (i.e., potential differences definitely caused by the injected current and not by background noise potentials) are used for further data inversion. From the monitoring results at Mölltaler Glacier and Magnetköpfl/Kitzsteinhorn, several different phases could be observed within the active layer. At first, during the autumn and early winter period, more and more brine channels got disconnected, resulting in a smooth, non-linear increase of resistivities (several 1000 to 10000 Ωm;). During this phase it can be assumed that ionic conductivity is still the governing part of conductivity due to the availability of enough free pore water inside connected channels. However, the available connected fluid phase is reduced successively, which is equivalent to a reduction of porosity. The results showed (Fig. 12) a non linear dependency between apparent resistivity and temperature ($\rho_{app} \propto \frac{1}{T^2}$) similar to Archie's law, provided that proportionality between temperature and porosity exists during this phase of freezing. We conclude that the effect of decreasing pore space is dominating the resistivity-temperature relation (compared to

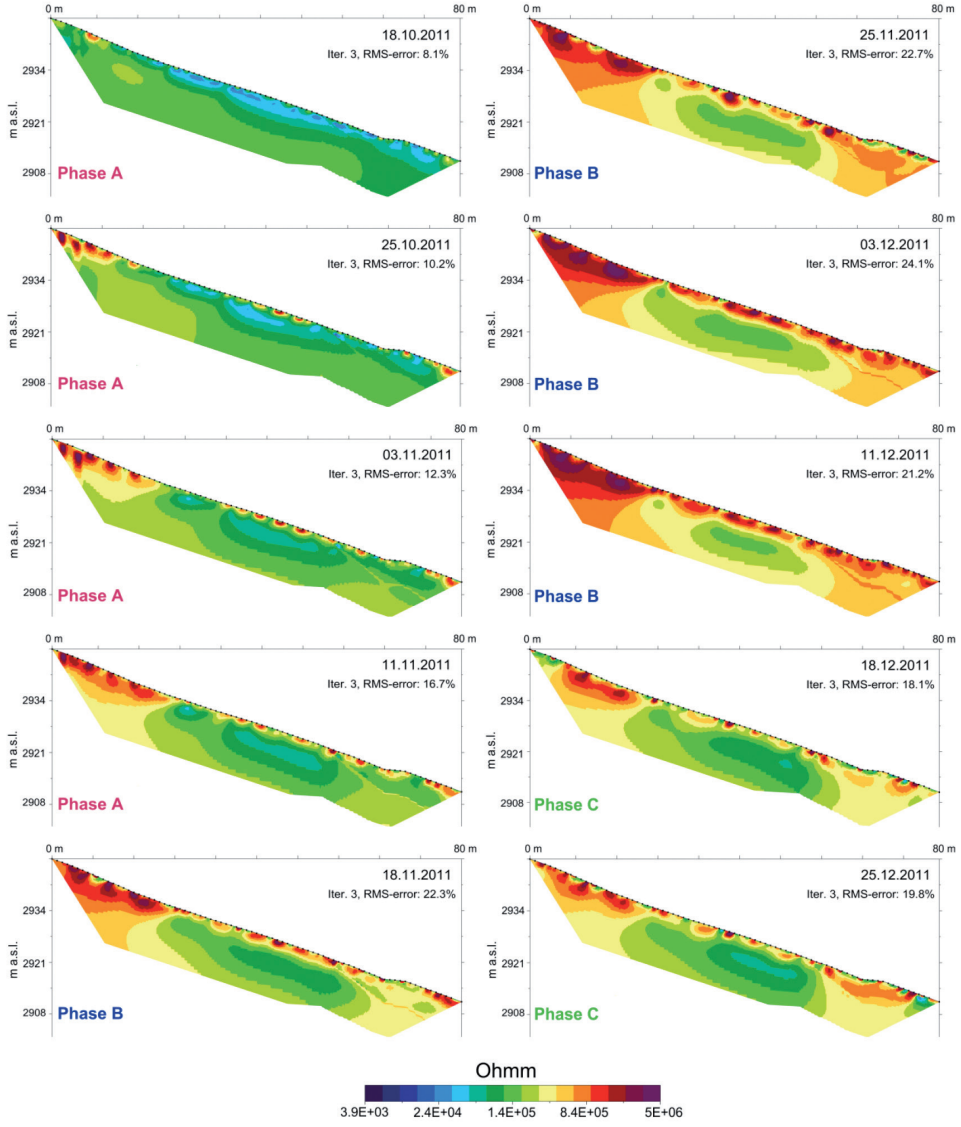

FIGURE 20
Selected inversion results covering the monitoring period from October 2011 to December 2011 measured at the monitoring site Magnetköpfl/Kitzsteinhorn; Phase indication corresponding to Fig. 16 is added to the inversion results.

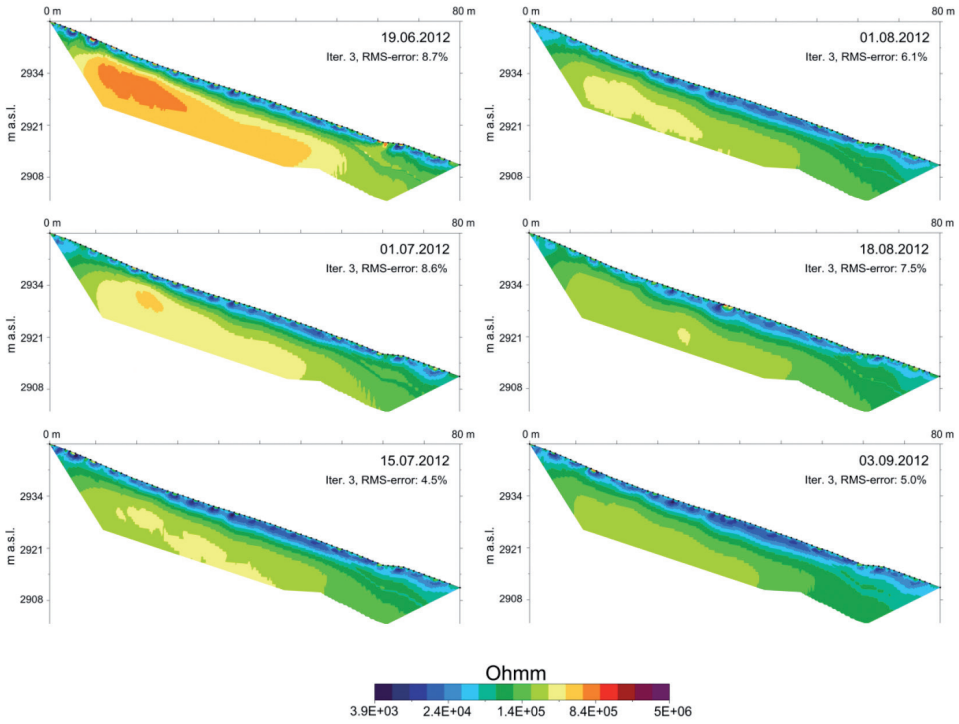

FIGURE 21
Selected inversion results covering the monitoring period from June 2012 to September 2012 at the monitoring site Magnetköpfl/Kitzsteinhorn.

decreased ion mobility) in this phase. This behaviour of values continues until a longer period of very low surface temperatures (–15 to –20°C), which cause a significant increase of subsurface resistivities (increasing from 10 kΩm to several 100 kΩm (Mölltaler Glacier) up to 3000 kΩm (Magnetköpfl/Kitzsteinhorn)) and a decrease of soil temperatures (below –6°C at 10 cm and –4°C at 0.8 m depth). After that event, electrical resistivity values start to vary intensively. In this period, average values of injected currents are very low between 0.01 and 0.02 mA (for example, see Fig. 18) and inversion errors are also comparably high (around 20%). It can be questioned whether the resolution of the used current sensor is good enough to accurately determine the values of such low injected currents. The measured high resistivities and big variations might suggest that hardly any continuous fluid-filled passages for ionic conduction are left due to the closure of connected brine channels.

At the test site of Magnetköpfl/Kitzsteinhorn, the results showed that soil temperature stayed constant for some time at the end of phase B and decreased (2°C) at the beginning of phase C, whereas apparent resistivity decreased again significantly from an average of 1000 kΩm to an average of 450 kΩm during this period (Fig. 16). Injected currents were also slightly increased. At the current state of our knowledge we could explain this behaviour by an increased dissociation of water due to an increased surface of the water-ice boundary layer (Murrmann 1973). However, this observation does not necessarily imply that temperature around the electrode (steel stakes) also stayed constant/ decreased. Figure 16 illustrates that the drop in apparent resistivity coincides with the time of snow events. If electrodes are not fully covered by snow we can assume that, since steel shows a good heat conductance, a local temperature minimum is induced. Thus the soil temperature around the electrode depends a lot on air temperature and might not be equal to the general soil temperature of the surface layer. Consequently, increased freezing around the electrodes is induced thus significantly increasing contact resistance. This could explain why apparent resistivity decreased again after different snow events at different positions along the profile. To verify such a process, however, would require a longer observation interval, video observations of the monitoring line and a more accurate current sensor.

During the spring period, resistivity monitoring clearly shows that the thawing process is very rapid and starts with the thawing of a shallow surface layer beneath a still closed snow cover, thus confirming the results from Hilbich *et al*. (2011). This effect increases the amount of current that can be injected at 400 V of applied voltage to more than 1 mA (Fig. 19). The resistivity of the active surface layer decreases down until 10 kΩm.

CONCLUSIONS AND OUTLOOK

In general, we can conclude that the developed monitoring technology provided high quality data to monitor freezing and thawing processes. In order to monitor changes even during winter times at soil temperatures below approximately –4.5°C, the accuracy of the current sensor still needs to be improved (an increase of the applied voltage for injection is not practicable in view of power efficiency). Several special problems of measurements at such low temperatures, which were described in the "Implications for permafrost monitoring" chapter, for example, the proper definition of the time delay window to avoid polariza-

tion effects and the eventual influences of Joule heating/cooling, were so far not adequately investigated. Measurements during such low temperature periods should be a special topic of further research, since hardly any monitoring field data is so far available for this temperature range. Here, further field studies, coupled with laboratory measurements, like those conducted by Krautblatter *et al*. (2010), but extending the temperature range to deeper values, might help to reveal further knowledge.

Forward modelling and subsequent inversion of derived data for the processes expected within the active layer (see Fig. 7) demonstrated that due to large resistivity variations in the shallow subsurface, calculation of resistivity values for deeper areas is still unreliable to a certain degree. This is also due to the possible latent ambiguities of geoelectrical inversion. Therefore, in this paper we did not focus much on the interpretation of resistivity changes at depth. For future application, the direct incorporation of statistically derived error estimates in the inversion routine, as suggested by Kim *et al*. (2010, 2013a, b), the use of 4D (Kim *et al*. 2009) and time lapse inversion (Loke *et al*. 2013) algorithms, as well as of alternative inversion technologies (e.g., Loke *et al*. 2003, Blaschek *et al*. 2008, Hermans *et al*. 2012, Kemna *et al*. 2002) promises a further increase of model accuracy and should be a target of future research.

From a practical point of view, the use of fuel cells has turned out to be reliable even under harsh conditions, if some basic rules for installation are followed. It can be concluded that they can provide enough power for monitoring a whole seasonal cycle without refuelling.

Finally, it has to be mentioned that an effect of temperature variations on the performance of the electronic components cannot be fully excluded. Therefore, the next version of the Geomon^{4D} equipment will also incorporate a device for temperature stabilization.

We also conclude that, although geoelectrical data acquisition and processing technology have improved significantly within recent years, so far data from only a few monitoring experiments of relatively short monitoring durations are available. However, to derive conclusions related to climate change, monitoring installations over several years or even decades need to be maintained at several locations. Given the frame of available sources of funding nowadays, which mainly envisage research periods of 3–4 years, such long term studies are hardly supported. Therefore, we hope that in future some funds are developed to make long term research possible.

ACKNOWLEDGEMENTS

The geoelectrical monitoring is supported by the project "TEMPEL – Temporal changes of geoelectrical properties as possible indicator of future failure of high risk landslides", funded by the Federal Ministry for Transport, Innovation and Technology and the Austrian Science Fund (FWF): TRP 175–N21 in frame of the Translational Brainpower Program, the FP7 project "SafeLand – Living with the landslide risk in Europe" and by internal funds of the Geological Survey of Austria. The pilot study at Sonnblick was partly financed in frame of the "ALPCHANGE – Climate Change and Impact in Southern Austrian alpine region" – project, supported by the Austrian Science Fund (P18304) and the Central Institute for Meteorology and Geodynamics (ZAMG). The soil temperature measurements at Kitzsteinhorn/Magnetköpfl are carried out in frame of the MOREXPERT project (alpS GmbH – Centre for Climate Change Adaptation Technologies and University of Salzburg). The borehole temperature data from Sonnblick and Fraganter Scharte were kindly provided by the Central Institute of Meteorology and Geodynamics, Vienna (ZAMG). We would further like to thank Gerhard Schauer (ZAMG), Sonnblick-Verein, Gletscherbahnen Kaprun AG and KELAG for their logistical and infrastructural support and I. Hartmeyer (University of Salzburg) for his involvement in performing the temperature monitoring at Magnetköpfl. We would like to thank Gerhard Kreuzer for the fruitful cooperation in implementing the electronic improvements for the GEOMON^{4D} system. In addition we want to thank the company KTS G.m.b.H. (P. Sporrer) for the support in operation and maintenance of the fuel cell system. SuperSting™, Sting™ and AGI EarthImager™ are trademarks of Advanced Geosciences, Inc. in the United States and in some other countries. EFOY is a protected trademark of SFC Energy AG. The authors thank two anonymous reviewers for their suggestions on an earlier version of the paper.

REFERENCES

Archie G.E. 1942. The electrical resistivity log as an aid in determining some reservoir characteristics. *Transactions of AIME* **146**(1), 54–62. doi: 10.2118/942054-G

Blaschek R., Hördt A. and Kemna A. 2008. A new sensitivity-controlled focusing regularization scheme for the inversion of induced polarization based on the minimum gradient support. *Geophysics* **73**(2), F45–F54. doi: 10.1190/1.2824820

Caranti J.M. and Illingworth A.J. 1983. Frequency Dependence of the Surface Conductivity of Ice. *Journal of Physical Chemistry* **87**, 4078–4083. doi:10.1021/j100244a016

Dahlin T. and Zhou B. 2004. A numerical comparision of 2D Resistivity imaging with 10 electrode arrays. *Geophysical Prospecting* **52**(5), 379–398. doi: 10.1111/j.1365-2478.2004.00423.x32

Davies M., Hamza O. and Harris C. 2003. Physical modelling of permafrost warming in rock slopes. *Proceedings of the 8th International Conference on Permafrost*, Zurich, Switzerland, 169–174.

De Koning M. and Antonelli A. 2007. On the Trapping of Bjerrum Defects in Ice Ih: The Case of the Molecular Vacancy. *Journal of Physical Chemistry B*, **111**(43), 12537–12542.

Derjaguin B.V. and Churaev N.V. 1978. The Theory of Frost Heaving. *Journal of Colloid Interface Sciences* **67**, 391–396.

Derjaguin B.V. and Churaev N.V. 1986. Flow of non-freezing water interlayers and frost heaving. *Cold Regions Science and Technology* **12**, 57–66.

Edwards S. 1976. A modified Pseudosection for Resistivity and IP. *Geophysics* **42**(5), 1020–1036.

French H.M, 1996. *The Periglacial Environment – Second Edition*. Harlow, Longman, 341.

Frolov A.D. 2003. A physical model of frozen ground considered as a complex macrosystem. *Proceedings of the 8th International Conference on Permafrost*, Zurich, Switzerland, 259–264.

Glen J.W. 1974. The physics of ice. USA Cold Regions Research and Engineering Laboratory, Monograph II-C2a.

Glen J.W. 1975. Mechanics of ice. USA Cold Regions Research and Engineering Laboratory, Monograph II-C2b.

Glen J.W. and Paren J.G. 1975. The electrical properties of snow and ice. *Journal of Glaciology* **15**(73), 15–38.

Grimm R.E., Stillman D.E., Dec S.F. and Bullock M.A. 2008. Low-Frequency Electrical Properties of Polycrystalline Saline Ice and Salt Hydrates. *Journal of Physical Chemistry B* **112**, 15382–15390.

Gruber S. and Haeberli W. 2007. Permafrost in steep bedrock slopes and its temperature-related destabilization following climate change. *Journal of Geophysical Research* **112**, F02S13.

Haeberli W., Hoelzle M. and Maisch M. 1998. Gletscher – Schlüsselindikatoren der globalen Klimaänderung. In: *Wissenschaftliche Fakten*, (eds J.L. Lozàn, H. Graszl and P. Hupfer). Warnsignal Klima, Hamburg, 213 p.

Haehnel R.B. 2001. Advances in ice control at corps hydraulic structures. *Ice Engineering* **31**.

Harris C., Davies M.C.R. and Etzelmueller B. 2001. The assessment of potential geotechnical hazards associated with mountain permafrost in a warming global climate. *Permafrost and Periglacial Processes* **12**, 145–156. doi: 10.1002/ppp.376

Hartmeyer I., Keuschnig M., Delleske R. and Schrott L. 2012. Reconstruction of the Magnetkoepfl rockfall event – Detecting rock fall release zones using terrestrial laser scanning, Hohe Tauern, Austria. *Geophysical Research Abstracts* **14**, EGU2012–12488.

Hauck C. 2002. Frozen ground monitoring using DC resistivity tomography. *Geophysical Research Letters* **29**(21).

Hauck C., Vonder Mühll D. and Maurer H. 2003. Permafrost monitoring using time-lapse resistivity tomography. *Proceedings of the 8th International Conference on Permafrost*, Zurich, Switzerland, 361–366.

Hauck C. and Kneisel C. 2006. Application of capacitively-coupled and DC electrical resistivity imaging for mountain permafrost studies. *Permafrost and Periglacial Processes* **17**, 169–177. doi: 10.1002/ppp. 555

Hausmann H., Supper R., Ita A., Römer A. and Mistelbauer T. 2010. The application of D.C. resistivity sounding in two Alpine ice caves. *Proceedings of the 4th International Workshop on Ice Caves*, June 5–11th, 2010, Obertraun, Austria.

Hermans T., Vandenbohede A., Lebbe L., Martin R., Kemna A., Beaujean J. *et al.* 2012. Imaging artificial salt water infiltration using electrical resistivity tomography constrained by geostatistical data. *Journal of Hydrology* **438–439**, 168–180. doi:10.1016/j.jhydrol.2012.03.021.

Hilbich C., Hauck C., Scherler M., Schudel L., Völksch I., Hoelzle M. *et al.* 2008. Monitoring mountain permafrost evolution using electrical resistivity tomography: A seven year study of seasonal, annual and long-term variations at Schilthorn, Swiss Alps. *Journal of Geophysical Research, Earth Surface* **113**, F01S90. doi:10.1029/2007JF000799.

Hilbich C., Marescot L., Hauck C., Loke M.H. and Mäusbacher R. 2009. Applicability of Electrical Resistivity Tomography Monitoring to Coarse Blocky and Ice-rich Permafrost Landforms. *Permafrost and Periglacial Processes* **20**(3), 269–284.

Hilbich C., Fuss C. and Hauck C. 2011. Automated time-lapse ERT for improved process analysis and monitoring of frozen ground. *Permafrost and Periglacial Processes* **22**(4), 306–319. doi: 10.1002/pp.732.

Hobbs P.V. 1974. *Ice Physics*. Oxford, United Kingdom: Clarendon Press.

Hoelzle M., Wagner S., Kääb A. and Vonder Mühll D. 1998. Surface movement and internal deformation of ice-rock mixtures within rock glaciers at Pontresina-Schafberg, Upper Engadin, Switzerland. *Proceedings of the 7th International Conference on Permafrost*, Yellowknife, Canada, 465–471.

Ikeda A., Matsuoka N. and Kääb A. 2003. A rapidly moving small rock glacier at the lower limit of mountain permafrost in the Swiss Alps. *Proceedings of the 8th International Conference on Permafrost*, Zurich, Switzerland, 455–460.

Jaccard C. 1959. Étude théorique et expérimentale des propriétés électriques de la glace. *Helvetica Physico Acta* **32**, 89–128.

Kamarov I.A. 2003. Effect of microscopic heterogeneities on water transfer in frozen ground, *Proceedings of the 8th International Conference on Permafrost*, Zurich, Switzerland, 579–583.

Kamarov I.A., Mironenko M.V. and Kiyashko N.V. 2012. Refinement of the standard basis for computational evaluation of thermophysical properties of saline soils and cryopegs. *Soil Mechanics and Foundation Engineering* **49**(2), 73–80.

Kemna A., Vanderborght J., Kulessa B. and Vereecken H. 2002. Imaging and characterisation of subsurface solute transport using electrical resistivity tomography (ERT) and equivalent transport models. *Journal of Hydrology* **267**(3–4), 125–146.

Keuschnig M., Hartmeyer I., Schmidjell A. and Schrott L. 2012. The adaptation of iButtons® for near-surface rock temperature and thermal offset measurements in a high alpine environment – Instrumentation and first results, Kitzsteinhorn (3203 m), Hohe Tauern, Austria. *Geophysical Research Abstracts* **14**, EGU2012–12981.

Khusnatdinov N.N., Petrenko V.F. and Levey C.G. 1997. Electrical Properties of the Ice/Solid Interface. *Journal of Physical Chemistry B* **101**, 6212–6214.

Kim J.H., Yi M.J., Park S.G. and Kim J.G. 2009. 4-D inversion of DC resistivity monitoring data acquired over a dynamically changing earth model. *Journal of Applied Geophysics* **68**, 522–532.

Kim, J.-H., Yi M.-J., Ahn H.-Y. and Kim K.-S. 2010. 4-D Inversion of Resistivity Monitoring Data Using L1 Norm Minimization. Paper presented at Near Surface 2010, A15, Zurich, Swiss.

Kim J.-H., Supper R., Tsourlos P. and Yi M.-J. 2013a. 4-D Inversion of Resistivity Monitoring Data Using L1 Norm Minimization. *Geophysical Journal International*, accepted.

Kim J.-H., Supper R., Jochum B., Ottowitz D. and Yi M.-J. 2013b. A new measurement protocol of DC resistivity data. *Geophysical Research Letters*, submitted.

Kneisel C., Hauck C., Fortier R. and Morrman B. 2008. Advances in Geophysical Methods for Permafrost Investigations. *Permafrost and Periglacial Processes* **19**, 157–178. doi: 10.1002/ppp.616

Koefoed O. 1979. *Geosounding Principles 1, Methods in Geochemistry and Geophysics 14A*. Elsevier.

Krautblatter M. and Hauck C. 2007. Electrical resistivity tomography monitoring of permafrost in solid rock walls. *Journal of Geophysical Research* **112**, F02S20. doi:10.1029/2006JF000546.

Krautblatter M., Verleysdonk S., Flores-Orozco A. and Kemna A. 2010. Temperature-calibrated imaging of seasonal changes in permafrost rock walls by quantitative electrical resistivity tomography (Zugspitze, German/Austrian Alps). *Journal of Geophysical Research, Earth Surface* **115**, F02003. doi:10.1029/2008JF001209.

Kroisleitner Ch., Reisenhofer S. and Schöner W. 2011. Chapter 2: Climate Change in the European Alps. In: *Thermal and geomorphic permafrost response to present and Future climate change in the European Alps*, (eds A. Kellerer-Pirklbauer *et al.*). APermaNET project, final report of Action 5.3. Online Publication, p.16–27. ISBN 978-2-903095-58-1

Kuras O., Meldrum P.I., Haslam E.P., Wilkinson P.B., Krautblatter M., Murton J.B. *et al.* 2011. Time-lapse Capacitive Resistivity Imaging – A Novel Methodology for the Monitoring of Permafrost Processes in Bedrock. *Near Surface 2011 – 17th European Meeting of Environmental and Engineering Geophysics*, Leicester, UK, 12–14 September 2011.

Laxton S. and Coates J. 2010. Geophysical and Borehole investigations of permafrost conditions associated with compromised infrastructure

in Dawson and Ross River, Yukon. In: *Yukon Exploration and Geology 2010*, (eds K.E. MacFarlane, L.H. Weston and C. Relfs). Yukon Geological Survey, p. 135–148.

Lewkowicz A.G., Etzelmueller B. and Smith S.L. 2011. Characteristics of Discontinuous Permafrost based on the Ground Temperature Measurements and Electrical Resistivity Tomography, Southern Yukon, Canada. *Permafrost and Periglacial Processes* **22**, 320–342. doi: 10.1002/ppp.703.

Loke M.H., Acworth I. and Dahlin T. 2003. A comparison of smooth and blocky inversion methods in 2D electrical imaging surveys. *Exploration Geophysics* **34**, 182–187.

Loke M.H., Dahlin T. and Rucker D.F. 2013. Smoothness-constrained time-lapse inversion of data from 3-D resistivity surveys. *Near Surface Geophysics* **12**(1).

Lukin Y.I., Mironov V.L. and Komarov S.A. 2008. Investigation of the Dielectric Spectra from Moist Soils During Freezing-Thawing Processes. *Russian Physics Journal* **51**(9), 907–911.

Marescot L., Loke M.H., Chapellier D., Delaloye R., Lambiel C. and Reynard E. 2003. Assessing reliability of 2D resistivity imaging in mountain permafrost studies using the depth of investigation index method. *Near Surface Geophysics* **1**(2), 57–67. doi: 10.3997/1873-0604.2002007

Matsuoka N., Ikeda A., Hirakawa K. and Watanabe T. 2003. Contemporary periglacial processes in the Swiss Alps: seasonal, inter-annual and long-term variations. *Proceedings of the 8th International Conference on Permafrost*, Zurich, Switzerland, p. 735–740.

Marion G.M. and Grant S.A. 1994. FREZCHEM: A Chemical-Thermodynamic Model for Aqueous Solutions at Subzero Temperatures. U.S: Army Cold Regions Research and Engineering Laboratory, Special Report 94–18.

Moore J.C. and Maeno N. 1993. Dielectric properties of frozen clay and silt soils. *Cold Regions Science and Technology* **21**, 265–273.

Murrmann R.P. 1973. Ionic Mobility in Permafrost. *Proceedings of the 2nd International Conference on Permafrost*. Yakutsk, Washington, D.C., National Academy of Sciences, p. 352–359.

Noetzli J., Hoelzle M. and Haeberli W. 2003. Mountain permafrost and recent Alpine rock-fall events: a GISbased approach to determine critical factors. *Proceedings of the 8th International Conference on Permafrost*, Zurich, Switzerland, 827–832.

Noetzli J., Hilbich C., Hauck C., Hoelzle M. and Gruber S. 2008. Comparison of Simulated 2D Temperature Profiles with Time-Lapse Electrical Resistivity Data at the Schilthorn Crest, Switzerland. *Proceedings of the 9th International Conference on Permafrost*. Institute of Northern Engineering, Fairbanks, Alaska, USA, 1293–1298.

Oldenborger G.A. 2010. Electrical Geophysics Applied to Assessing Permafrost Conditions in Pangnirtung, Nunavut. Geological Survey of Canada, Open File 6725, 39 p.

Oldenburg D.W. and Li Y.G. 1999. Estimating depth of investigation in dc resistivity and IP surveys. *Geophysics* **64**(2), 403–416.

Petrenko V. 1993. Electrical Properties of Ice, Special Report 93–20, U.S.Army Cold Regions Research, New Hampshire.

Petrenko V.F. and Ryzhkin I.A. 1997. Surface States of Charge Carriers and Electrical Properties of the Surface Layer of Ice. *Journal of Physical Chemistry B* **101**, 6285–6289.

Petrenko V. and Qi S. 1999. Reduction of ice adhesion to stainless steel by ice electrolysis. *Journal of Applied Physics* **86** (19), 5450–5454.

Petrenko V. F. and Whitworth R. W. 1999. *The Physics of Ice*. Oxford University Press, 384 pp. ISBN 0-19851-895-1.

Petrenko V. and Courville Z. 2000. Active de-icing coating for aerofoils. *Proceedings of the 38th Aerospace Science Meeting and Exhibition*, Reno, Nevada.

Petrenko V.F. and Ryzhkin I.A. 2011. Non-Joule Heating of Ice in an Electric Field. *Journal of Physical Chemistry A* **115**, 6202–6207.

Ribolini A. and Fabre D. 2007. Shallow active layer temperature and DC resistivity of a rock glacier in the Argentera Massif, Maritime Alps, Italy. *Zeitschrift für Geomorphologie, Supplementbände* **51**(2), 55–77.

Rödder T. and Kneisel C. 2012. Permafrost mapping using quasi-3D resistivity imaging, Murtèl, Swiss Alps. *Near Surface Geophysics* **10**(2), 117–127. doi: 10.3997/1873-0604.2011029

Sass O. 2004. Rock moisture fluctuations during freeze-thaw cycles: Preliminary results from electrical resistivity measurements. *Polar Geography* **28**(1), 13–31.

Schneider S., Hauck C. and Hoelzle M. 2011. Geophysical monitoring of different permafrost forms within the Murtèl- Corvatsch Area, Upper Engadin. *Proceedings of the 9th Swiss Geoscience Meeting*, Open Cryosphere Session.

Slater L., Binley A., Daily W. and Johnson R. 2000. Crosshole electrical imaging of a controlled saline tracer injection. *Journal of Applied Geophysics* **44**, 85–102.

Smith M.W. 1993. Climatic change and permafrost. In: *Canada's Cold Environments*, (eds H.M. French and O. Slaymaker). Montreal: McGill-Queen's University Press, 291–311.

Stillman D.E., Grimm R.E. and Dec S.F. 2010. Low-Frequency Electrical Properties of Ice-Silicate Mixtures. *Journal of Physical Chemistry B* **114**, 6065–6073.

Supper R. and Römer A. 2003. New Achievements in Developing a High Speed Geoelectrical Monitoring System for Landslide Monitoring. *Proceedings of the 9th Environmental and Engineering Geophysical Society Meeting*, Prague.

Supper R. and Römer A. 2004. New Achievements in Developing a High Speed Geoelectrical Monitoring System for Landslide Monitoring (GEOMONITOR2D). *Proceedings of the SAGEEP 2004 Meeting*, Colorado Springs.

Supper R., Römer A., Bieber G. and Jaritz W. 2005. A Complex Geoscientiffic Strategy for Landslide Hazard Mitigation – Case Study Sibratsgfäll. *Proceedings of Near Surface Geophysics Conference*, Palermo.

Supper R., Ahl A., Römer A., Jochum B. and Bieber G. 2007a. A complex geo-scientific strategy for landslide hazard mitigation – from airborne mapping to ground monitoring. *Advances in Geosciences* **14**, 1–6.

Supper R., Ita A., Römer A., Jochum B. and Ottowitz D. 2010. Geomon^{4D} – a new high speed tool for geoelectrical monitoring in permafrost regions. *Proceedings of the Permafrost Workshop Obergurgl*, 14–15 Oktober.

Vanhala H., Lintinen P. and Ojala A. 2009. Electrical Resistivity Study of Permafrost on Ridnitšohkka Fell in Northwest Lapland, Finland. *Geophysica* **45**(1–2), 103–118.

Wolff E.W., Miners W.D., Moore J.C. and Paren J.G. 1997. Factors controlling the electrical conductivity of ice from polar regions – a summary. *Journal of Physical Chemistry B* **101**(32), 6090–6094.

Zimmermann M. and Haeberli W. 1992. Climatic change and debris flow activity in high-mountain areas – a case study in the Swiss Alps. *Catena Supplement* **22**, 59–72.